Pyrrole and Pyridine Peripherally Fused Perylene: Columnar Packing, Anti-kasha Dual Emission and Reactive Oxygen Species Generation

(Supporting Information)

Jing Cao,[a] Wenhao Zhang,[a] Yeda Ding,[a] Xuejin Zhang,[a] Yuanyuan Zhang,[a] Dan Qiao,[a] Shumin Biao,[a] Xuefei Dong,[a] Jiayi Song,[a] Gaole Dai,*[b] Ruiguo Zhao,*[a] Qing Wang*[a]

[a] School of Chemistry and Chemical Engineering, Inner Mongolia University, 235 West University Street, Hohhot 010021, China

Email: zhaoruig@imu.edu.cn qingwang@imu.edu.cn

[b] College of Material Chemistry and Chemical Engineering, Key Laboratory of Organosilicon Chemistry and Material Technology, Ministry of Education, Hangzhou Normal University, Hangzhou 311121, Zhejiang, P. R. China

Email:daigaole@ hznu.edu.cn

1. Experimental Section

Table of Contents

1.1 General

All reagents were purchased from commercial sources without further purification. ^{1}H and ^{13}C NMR spectra were recorded using Bruker Advance II 500 MHz or 600 MHz spectrometer in $CDCl_3$ or MeOD with tetramethylsilane (TMS) as the internal standard. The chemical shift was recorded in ppm and the following abbreviations were used to explain the multiplicities: s = singlet, d = doublet, t = triplet, m = multiplet, br = broad. APCI and ESI mass spectra were recorded on a SHIMADZU/LCMS-IT-TOF instrument. UV-Vis-NIR absorption was recorded on a SHIMADZU UV-2600i spectrophotometer. Steady-state photoluminescence (PL) spectra were recorded on a HITACHI F-4700 spectrophotometer. Absolute PL quantum yield was measured on a HAMAMATSU C11347-11 spectrometer. Cyclic voltammetry measurements were performed in dry dichloromethane (DCM) and tetrahydrofuran (THF) on a CHI 620C electrochemical analyzer with a three-electrode cell, using 0.1 M Bu_4NPF_6 as supporting electrolyte, AgCl/Ag as reference electrode, gold disk as working electrode (2 mm diameter, polished with a polishing cloth containing Al_2O_3 powder (particle size 0.05 um)), Pt as counter electrode. Analyte concentration is $7*10^{-4}$ M, and the solution was deaerated with bubbling argon prior measurement. The initial potential is 0.00 V, and sweeps in a positive direction with a scan rate of 100 mV/s at room temperature. Potential was externally calibrated against the ferrocene/ferrocenium couple. The single

crystal was measured at low temperature (T = 193 K) on a Bruker D8 VENTURE Metaljet PHOTON II diffractometer. IR spectra were recorded on Thermo Scientific Nicolet iS20. Melting points were determined with melting points apparatus and are uncorrected.

1.2 Synthetic procedures and characterization data

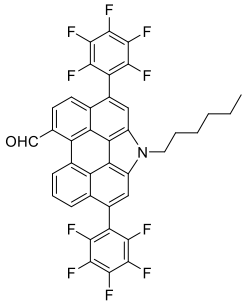

NP-CHO

To a suspension of **NP** [1] (500 mg, 0.73 mmol) in dry CH_2Cl_2 (15 mL), $SnCl_4$ (0.26 mL, 2.22 mmol) was added in one portion at 0°C under argon atmosphere, and then Cl_2CHOCH_3 (0.2 mL, 2.21 mmol) was added dropwise over 1 h. The reaction mixture was stirred for additional 1 h at 0°C and then slowly warmed up to room temperature and then refluxed for 3 h. After cooling, water (100 mL) was added to quench the reaction and the organic layer was separated, washed by water, and dried over sodium sulfate. Solvent was removed under vacuum, and the residue was purified by column chromatography (silica gel, hexane/ethyl acetate = 20:1 v/v R_f = 0.30) to afford the pure product **NP-CHO** as orange solid (260 mg, 50% yield); ^{1}H NMR (600 MHz, $CDCl_3$) δ (ppm) = 11.06 (s, 1H), 8.50 (d, J = 7.3 Hz, 1H), 8.35 (d, J = 8.5 Hz, 1H), 8.04 (s, 1H), 7.99 – 7.93 (m, 3H), 7.87 (d, J = 8.6 Hz, 1H), 4.83 (t, J = 7.1 Hz, 2H), 2.19 – 2.14 (m, 2H), 1.47 – 1.42 (m, 2H), 1.38 – 1.33 (m, 2H), 1.30 – 1.24 (m, 2H), 0.83 (t, J = 7.3 Hz, 3H); ^{13}C NMR (151 MHz, $CDCl_3$) δ (ppm) = 192.06, 145.01 (d, $J_{F\text{-}C}$ = 255.4 Hz), 141.18 (d, $J_{F\text{-}C}$ = 255.4 Hz), 138.01 (d, $J_{F\text{-}C}$ = 251.0 Hz), 132.93, 132.78, 132.52, 131.89, 130.54, 129.59, 128.38, 127.26, 125.78, 125.00, 124.95, 124.69, 123.04, 121.88, 120.37, 118.06, 117.98, 117.79, 116.52, 114.84 (d, $J_{F\text{-}C}$ = 38.7, 18.9 Hz), 46.24, 31.37, 31.25, 26.94, 22.48, 13.85. 35 carbons are expected, but 30 carbons show up in C-NMR spectrum, which maybe ascribe to signal overlap or low intensity due to F coupling. IR (KBr, cm^{-1}) 2929.87, 2855.33, 1681.86, 1548.09, 1523.50, 1492.09, 1370.04, 1355.74, 1307.03, 1260.52, 1214.35, 1184.81, 1105.49, 1082.58, 1018.21, 1005.18, 983.19, 903.65, 875.65, 793.04, 776.42, 761.69, 721.97, 663.24. mp 165℃. HRMS (APCI, positive mode): m/z $(M+H)^+$ calcd for $C_{39}H_{21}F_{10}NO$ 710.1541; found: 710.1538 (error: -0.42 ppm).

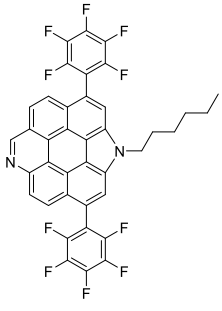

PerNN

Trifluoroacetic acid (TFA) (1.0 mL), azidotrimethylsilane ($TMSN_3$) (1.14 g, 9.89 mmol) and trifluoromethanesulfonic acid (TfOH) (0.68 g, 4.52 mmol) were added sequentially into a 25 mL two-neck flask containing **NP-CHO** (50 mg, 0.07 mmol) under air. The resulting solution was stirred in oil bath at 60°C for 1 h. The reaction mixture was then diluted with ethyl acetate, washed with aqueous NaOH (2 M, 5 mL), and dried over anhydrous Na_2SO_4. Solvents were removed under vacuum. The crude product was further purified by flash column chromatography (silica gel, hexane/ethyl acetate = 6:1 v/v R_f = 0.45) to give powder compound **PerNN** as faint yellow solid (19.05 mg, 38% yield); ^{1}H NMR (600 MHz, $CDCl_3$) δ (ppm) = 10.28 (s, 1H), 8.86 (d, J = 8.4 Hz, 1H), 8.71 (d, J = 8.8 Hz, 1H), 8.51 (d, J = 8.5 Hz, 1H), 8.48 (s, 1H), 8.41 (s, 1H), 8.39 (d, J = 9.1 Hz, 1H), 5.06 (t, J = 6.8 Hz, 2H), 2.35 – 2.30 (m, 2H), 1.56 – 1.51 (m, 2H), 1.42 – 1.37 (m, 2H), 1.31 – 1.28 (m, 2H), 0.84 (t, J = 7.2 Hz, 3H); ^{13}C NMR (151 MHz, $CDCl_3$) δ (ppm) = 149.82, 144.98 (d, J_{F-C} = 246.5 Hz), 143.98, 141.21 (d, J_{F-C} = 256.7 Hz), 138.09 (d, J_{F-C} = 252.7 Hz), 135.89, 135.47, 126.39, 125.99, 124.90, 124.02, 123.72, 122.89, 121.71, 120.70, 120.45, 119.66, 118.70, 118.33, 116.22, 115.30 (d, J_{F-C} = 15.9 Hz), 114.85, 47.03, 31.43, 31.22, 27.01, 22.48, 13.88. 35 carbons are expected, but 28 carbons show up in C-NMR spectrum, which maybe ascribe to signal overlap or low intensity due to F coupling. IR (KBr, cm^{-1}) 2929.36, 2856.15, 1689.06, 1650.38, 1595.73, 1562.11, 1521.52, 1485.63, 1453.73, 1406.89, 1336.62, 1314.96, 1294.08, 1100.48, 1051.70, 1013.03, 986.32, 899.25, 866.81, 826.42, 813.10, 792.68, 726.62, 660.07, 490.31. mp 225℃. HRMS (APCI, positive mode): m/z $(M+H)^+$ calcd for $C_{39}H_{20}F_{10}N_2$ 707.1545 ; found: 707.1530 (error: -2.12 ppm).

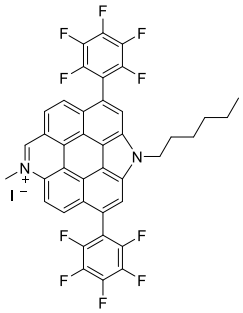

PerNN-MeI

PerNN (20 mg, 0.028 mmol) was dissolved in dry MeCN (1 mL) and heated to 90°C for 0.5 h under nitrogen atmosphere until it was fully dissolved. Iodomethane (1 mL, 16.1 mmol) was subsequently added, and the reaction mixture was stirred at 9°C for overnight. After being cooled to room temperature, the solvent was removed by evaporation, and the residue was purified by flash column chromatography (silica gel, DCM/methyl alcohol = 20:1 v/v R_f = 0.14) to give powder compound **PerNN-MeI** as yellow solid (16.14 mg, 79% yield); ^{1}H NMR (600 MHz, MeOD) δ (ppm) = 10.69 (s, 1H), 9.24 (s, 1H), 9.14 - 9.12 (m, 3H), 9.05 (d, J = 8.9 Hz, 1H), 8.86 (d, J = 8.7 Hz, 1H), 5.35 (t, J = 6.6 Hz, 2H), 5.29 (s, 3H), 2.40 – 2.35 (m, 2H), 1.50 – 1.44 (m, 2H), 1.40 – 1.35 (m, 2H), 1.30 – 1.28 (m, 2H), 0.77 (t, J = 7.2 Hz, 3H); ^{13}C NMR (151 MHz, MeOD) δ (ppm) = 147.57, 145.11 (d, J_{F-C} = 240.0 Hz), 141.75 (d, J_{F-C} = 262.0 Hz), 138.12 (t, J_{F-C} = 127.4 Hz), 137.81, 136.21, 135.02, 131.03, 128.26, 127.17, 124.22, 122.83, 122.52, 122.14, 120.86, 118.58, 118.24, 118.08, 117.50, 117.01, 116.74, 114.89, 114.03 (t, J_{F-C} = 18.6 Hz), 114.03, 45.13, 31.09, 30.92, 26.46, 22.09, 12.69. 36 carbons are expected, but 30 carbons show up in C-NMR spectrum, which maybe ascribe to signal overlap or low intensity due to F coupling. IR (KBr, cm^{-1}) 2920.90, 2850.79, 1730.30, 1686.88, 1652.39, 1599.33, 1576.69, 1522.77, 1496.59, 1453.94,

1380.94, 1336.91, 1317.04, 1294.38, 1262.02, 1214.33, 1180.40, 1154.90, 1098.72, 1051.82, 1031.09, 1013.26, 988.05, 878.05, 817.09, 790.99, 744.56, 681.30, 665.22, 638.12, 577.52, 491.03. mp 166℃. HRMS (ESI, positive mode): m/z M^+ calcd for $C_{40}H_{23}F_{10}N_2^+$ 721.1696 ; found: 721.1675 (error: -2.91 ppm).

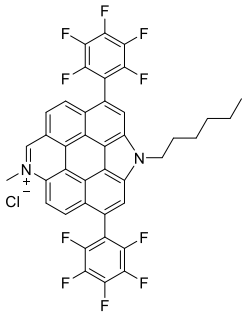

PerNN-MeCl

PerNN-MeI (16.14 mg, 0.022 mmol) solid was redissolved in methnol (3 mL). Aqueous solution (0.5 mL) of NH_4PF_6 (17.93 mg, 0.11 mmol.) was added followed by addition of water (5 mL). The resulting precipitate was filtrated, dried and redissolved in MeCN (1.2 mL). A MeCN solution (0.5 mL) of tetrabutylammonium chloride (30.57 mg, 0.11 mmol.) was added, and the reaction mixture was stirred 1 min. After reaction completion, solvent was removed by evaporation. The crude product was purified by flash column chromatography (silica gel, DCM/methnol = 20:1 v/v R_f = 0.15) to give oily curde product. The oil mixture was then dissolved in DCM, and the organic layer was separated and washed by water, dried over sodium sulfate. Finally, solvent was removed under vacuum, and the residue was washed by hexane to give **PerNN-MeCl** as yellow solid (12.11 mg, 75% yield); ^{1}H NMR (600 MHz, $CDCl_3$) δ (ppm) = 12.52 (s, 1H), 9.42 (d, J = 8.4 Hz, 1H), 8.96 (m, 2H), 8.81 (s, 1H), 8.72 (s, 1H), 8.69 (d, J = 8.1 Hz, 1H), 5.66 (s, 3H), 5.20 (t, J = 6.8 Hz, 2H), 2.43 – 2.35 (m, 2H), 1.66 – 1.61 (m, 2H), 1.44 – 1.39 (m, 2H), 1.31 – 1.29 (m, 2H), 0.84 (d, J = 7.2 Hz, 3H); ^{13}C NMR (126 MHz, $CDCl_3$) δ (ppm) = 150.32, 144.86 (d, J_{F-C} = 243.6 Hz), 141.80 (d, J_{F-C} = 252.7 Hz), 138.22 (d, J_{F-C} = 255.8 Hz), 137.59, 135.97, 134.55, 130.97, 128.43, 127.56, 127.18, 126.23, 124.14, 122.91, 122.81, 122.61, 119.90, 118.87, 118.57, 118.18, 117.80, 117.62, 117.41, 114.61, 113.79 (d, J_{F-C} = 2.1 Hz), 45.84, 31.38, 31.34, 27.02, 22.44, 13.86. 36 carbons are expected, but 31 carbons show up in C-NMR spectrum, which maybe ascribe to signal overlap or low intensity due to F coupling. IR (KBr, cm^{-1}) 2922.25, 2852.03, 1655.58, 1602.04, 1522.88, 1494.81, 1379.42, 1317.13, 1294.61, 1263.32, 1212.91, 1153.17, 1099.67, 1014.54, 986.90, 883.60, 819.61, 789.33, 683.67, 583.35, 488.95. mp 148℃. HRMS (ESI, positive mode): m/z M^+ calcd for $C_{40}H_{23}F_{10}N_2^+$ 721.1696 ; found: 721.1689 (error: -0.97 ppm).

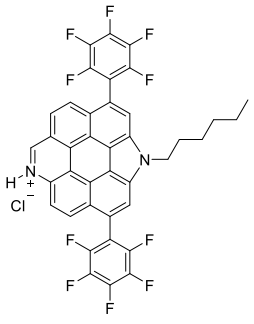

PerNN-H

PerNN (20 mg, 0.028 mmol) was dissolved in DCM (1 mL) and 2.6 ul HCl (12 M) was added dropwise, and the reaction mixture was stirred for 30 min. After reaction

completion, solvent was removed by evaporation, and the residue was washed by hexane to give compound **PerNN-H** as yellow solid (20 mg, 100% yield); ^{1}H NMR (600 MHz, $CDCl_3$) δ (ppm) = 10.43 (s, 1H), 9.00 (d, *J* = 8.9 Hz, 1H), 8.78 (d, *J* = 8.9 Hz, 1H), 8.67 (s, 1H), 8.63 (d, *J* = 8.9 Hz, 1H), 8.56 (s, 1H), 8.53 (d, *J* = 8.8 Hz, 1H), 5.15 (t, *J* = 6.9 Hz, 2H), 2.38 – 2.32 (m, 2H), 1.56 – 1.51 (m, 2H), 1.43 – 1.38 (m, 2H), 1.32 – 1.28 (m, 2H), 0.84 (t, *J* = 7.2 Hz, 3H); ^{13}C NMR (151 MHz, $CDCl_3$) δ (ppm) = 160.41, 144.94 (d, J_{F-C} = 243.7 Hz), 142.37, 138.11 (d, J_{F-C} = 125.2 Hz), 137.78, 136.46, 133.81, 131.25, 129.73, 127.50, 127.31, 124.70, 124.62, 123.15, 122.75, 122.09, 119.97, 118.58, 118.29, 117.89, 117.57, 117.23, 115.39, 113.50, 112.97 (d, J_{F-C} = 165.2 Hz), 47.62, 31.33, 27.01, 22.43, 13.80. 35 carbons are expected, but 30 carbons show up in C-NMR spectrum, which maybe ascribe to signal overlap or low intensity due to F coupling. IR (KBr, cm^{-1}) 2924.82, 2851.59, 1730.35, 1690.45, 1597.94, 1522.94, 1485.50, 1383.77, 1338.01, 1317.95, 1295.85, 1196.88, 1140.18, 1101.01, 1052.92, 1013.86, 987.81, 899.28, 877.46, 812.60, 793.08, 753.77, 719.36, 688.79, 662.02, 611.07, 580.29, 553.57, 489.96. HRMS (ESI, positive mode): m/z M^+ calcd for $C_{39}H_{21}F_{10}N_2^+$ 707.1540 ; found: 707.1550 (error: 1.41 ppm).

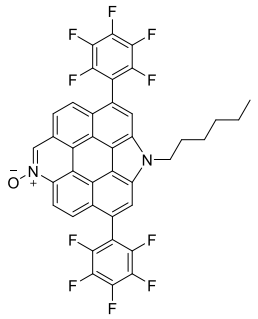

PerNN-O

m-Chloroperbenzoic acid (m-CPBA) (19.55 mg, 0.11 mmol) was added in a solution of **PerNN** (20 mg, 0.028 mmol) in CH_2Cl_2 (2.3 mL) at 0°C. The reaction mixture was stirred for 90 min at 0 °C, then stirred at room temperature for overnight. After being concentrated under reduced pressure, the crude product was purified by flash column chromatography (silica gel, DCM/methnol = 30:1 v/v R_f = 0.33) to give **PerNN-O** as yellow solid (11.25 mg, 55% yield); ^{1}H NMR (600 MHz, $CDCl_3$) δ (ppm) = 9.78 (s, 1H), 9.22 (d, *J* = 9.2 Hz, 1H), 8.50 (d, *J* = 9.2 Hz, 1H), 8.44 (s, 1H), 8.43 – 8.42 (m, 2H), 8.35 (d, *J* = 8.8 Hz, 1H), 5.06 (t, *J* = 7.1 Hz, 2H), 2.34 – 2.29 (m, 2H), 1.56 – 1.50 (m, 2H), 1.42 – 1.39 (m, 2H), 1.31 – 1.29 (m, 2H), 0.84 (t, *J* = 7.3 Hz, 3H); ^{13}C NMR (151 MHz, $CDCl_3$) δ (ppm) = 144.91 (d, J_{F-C} = 247.3 Hz), 141.32 (d, J_{F-C} = 245.6 Hz), 137.85 (d, J_{F-C} = 125.9 Hz), 137.35, 135.80, 135.75, 135.44, 126.63, 125.81, 124.68, 123.87, 123.79, 121.77, 121.65, 121.46, 119.81, 119.54, 119.37, 119.23, 118.31, 117.78, 116.89, 116.24, 115.92, 114.90 (d, J_{F-C} = 17.4 Hz), 47.15, 31.40, 31.25, 29.70, 22.47, 13.87. 35 carbons are expected, but 31 carbons show up in C-NMR spectrum, which maybe ascribe to signal overlap or low intensity due to F coupling. IR (KBr, cm^{-1}) 2922.62, 2851.68, 1688.44, 1650.10, 1595.32, 1565.05, 1521.30, 1487.81, 1401.43, 1338.34, 1303.21, 1262.46, 1188.37, 1105.67, 1083.89, 1051.61, 1012.55, 987.40, 869.47, 818.76, 790.71, 672.53, 627.84, 490.41. mp 133°C. HRMS (ESI, positive mode): m/z $(M+H)^+$ calcd for $C_{39}H_{20}F_{10}N_2O$ 723.1494 ; found: 723.1488 (error: -0.83 ppm).

2. Reactive oxygen species (ROS)

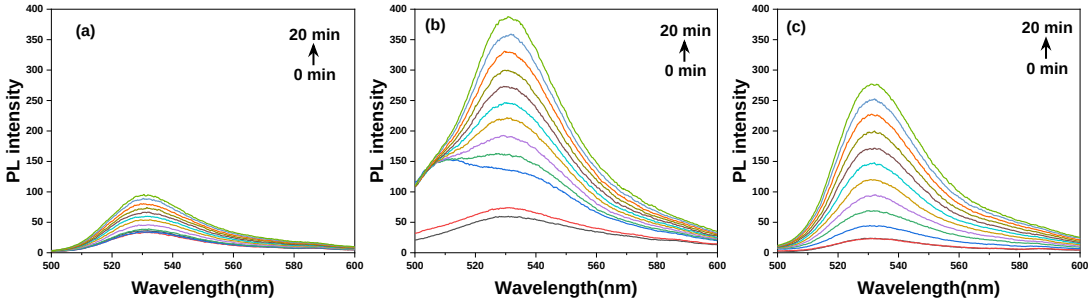

Figure S1. The fluorescence spectra changes of DCFH for ROS detection. (a) DCFH alone, (b) **PerNN**+DCFH and (c) **PerNN-O**+DCFH under white light with different irradiation time. Concentration of **PerNN** or **PerNN-O** is 10^{-5} M; Light power: 180 mW cm^{-2}.

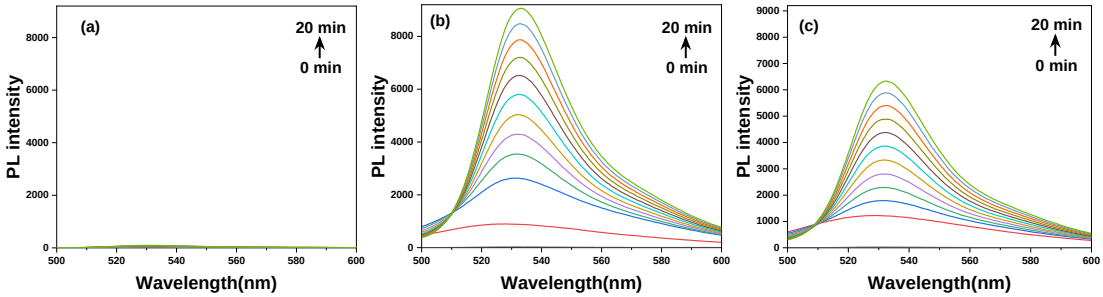

Figure S2. The fluorescence spectra changes of DCFH for ROS detection. (a) DCFH alone, (b) **PerNN-MeI**+DCFH and (c) **PerNN-MeCl**+DCFH under white light with different irradiation time. Concentration of **PerNN-MeI** or **PerNN-MeCl** is 10^{-5} M; Light power: 180 mW cm^{-2}.

3. Photoelectrical properties

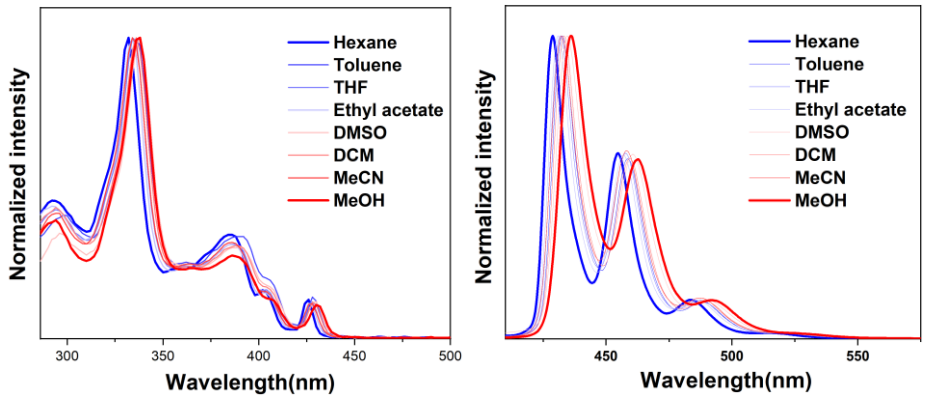

Figure S3. UV–vis absorption (left; 10^{-5} M) and emission (right; 10^{-5} M; excitation with 430 nm) spectra of **PerNN** in different solvents.

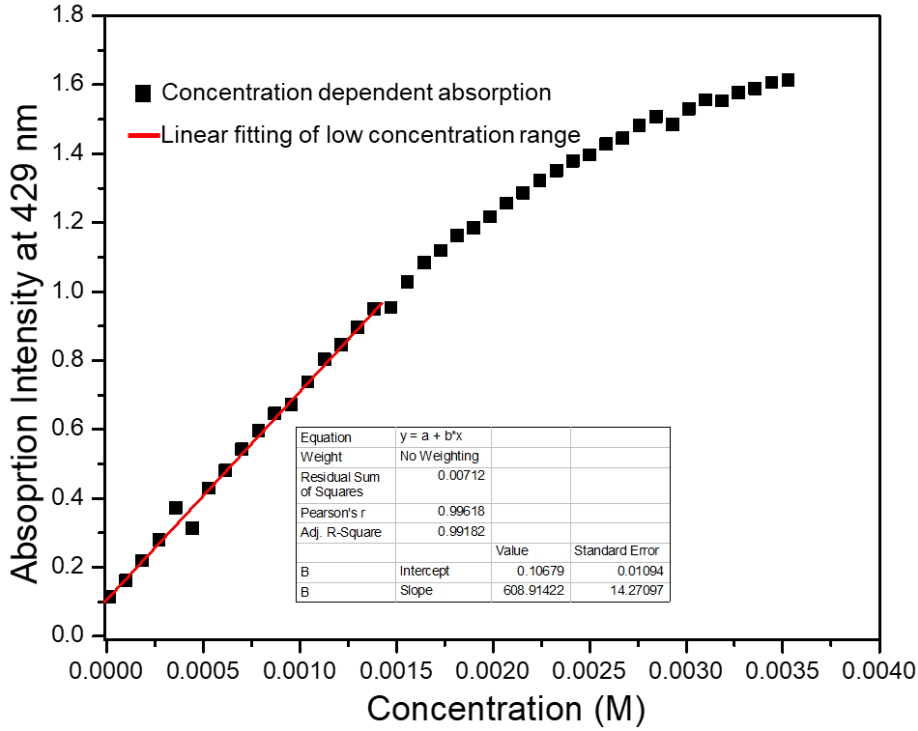

Figure S4. Concentration-dependent absorption intensity at 429 nm of **PerNN** in toluene.

Table S1. Summarize the photophysical properties of **PerNN** in different solvents.

Solvent	**Hexane**	**Toluene**	**THF**	**Ethyl acetate**	**DMSO**	**DCM**	**MeCN**	**MeOH**	**Powder**
λ_{abs}/nm	425	427	427	425	429	427	427	429	
λ_{em}/nm	428	432	432	431	434	434	432	437	
QY(%)	17.10	25.94	22.6	20.6	30.64	21.80	21.86	24.62	3.82

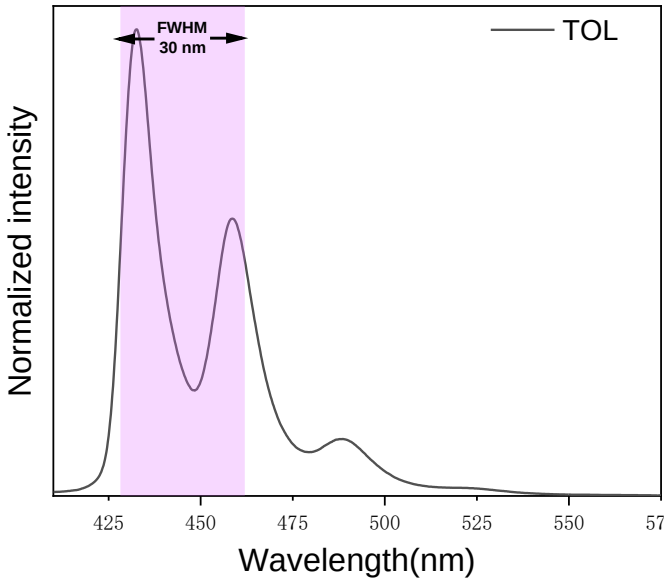

Figure S5. Full width at half maximum (FWHM) of **PerNN** in toluene.

Table S2. Full width at half maximum (FWHM) of **PerNN** in different solvents.

solvent	**THF**	**Ethyl acetate**	**MeOH**	**DMSO**	**Toluene**	**DCM**	**MeCN**	**Hexane**
FWHM(nm)	30	30	32	31	30	31	31	30

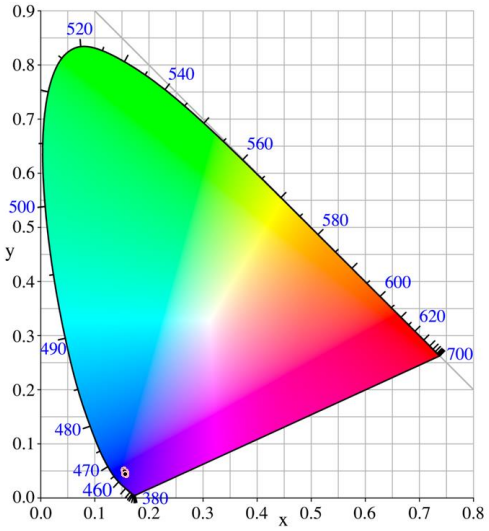

Figure S6. Fluorescent color coordinates in CIE 1931 chromaticity diagrams of **PerNN** in different solvents.

Table S3. Fluorescent color coordinates of **PerNN** in different solvents.

solvent	CIE x	CIE y
Toluene	0.1547	0.044
Hexane	0.1575	0.0424
MeCN	0.1558	0.047
DCM	0.1552	0.0479
MeOH	0.1534	0.0522
THF	0.1569	0.0476
DMSO	0.1545	0.0492
Ethyl acetate	0.156	0.0445

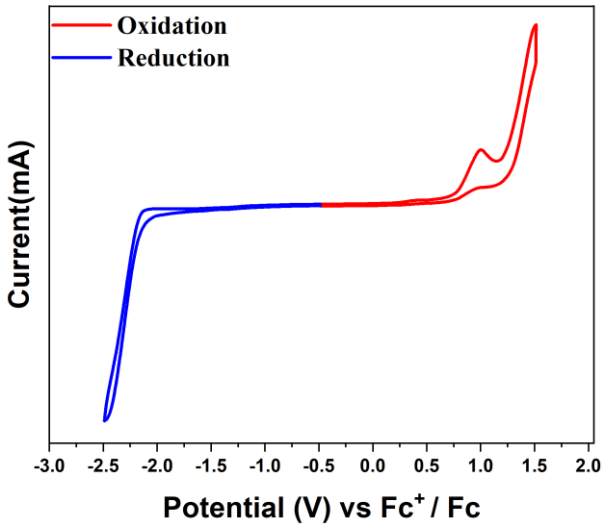

Figure S7. Cyclic voltammogram of **PerNN** in DCM with 0.1 M Bu_4NPF_6 as a supporting electrolyte.

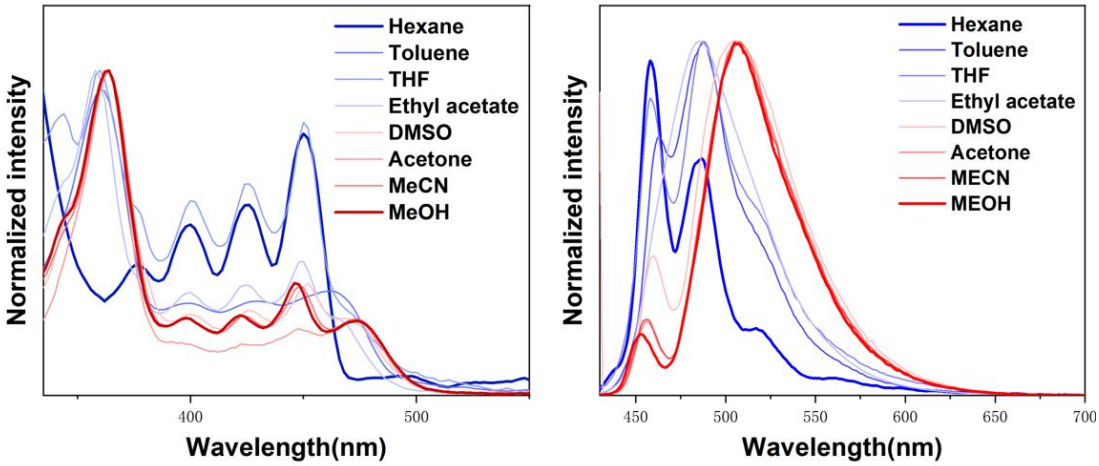

Figure S8. UV–vis absorption (left; 10^{-5} M) and emission (right; 10^{-5} M; excited with 420 nm) spectra of **PerNN-MeI** in different solvents.

Table S4. Summarize the photophysical properties of **PerNN-MeI** in different solvents.

Solvent	**Hexane**	**Toluene**	**THF**	**Ethyl acetate**	**DMSO**	**Acetone**	**MeCN**	**MeOH**	**Powder**
λ_{abs}/nm	450	463	450	466	470	472	474	474	
λ_{em}/nm	458	488	488	486	507	507	506	506	
QY(%)	53.32	52.26	62.28	47.56	52.12	24.42	32.38	35.26	0.91

Note: λ_{em} denotes the maximum emission wavelength.

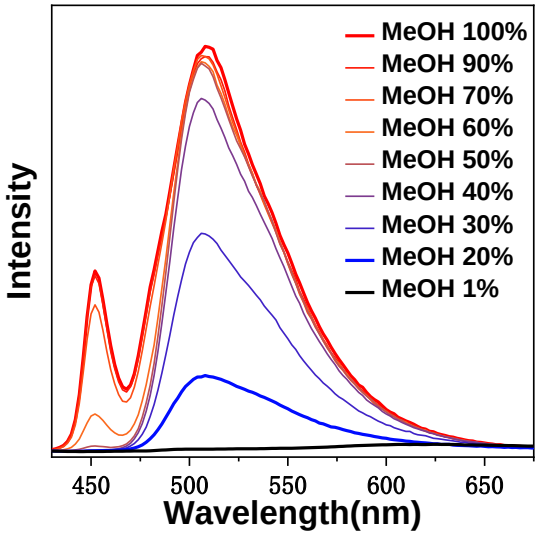

Figure S9. Emission spectra of **PerNN-MeI** in MeOH/water mixed solvents with different MeOH fraction.

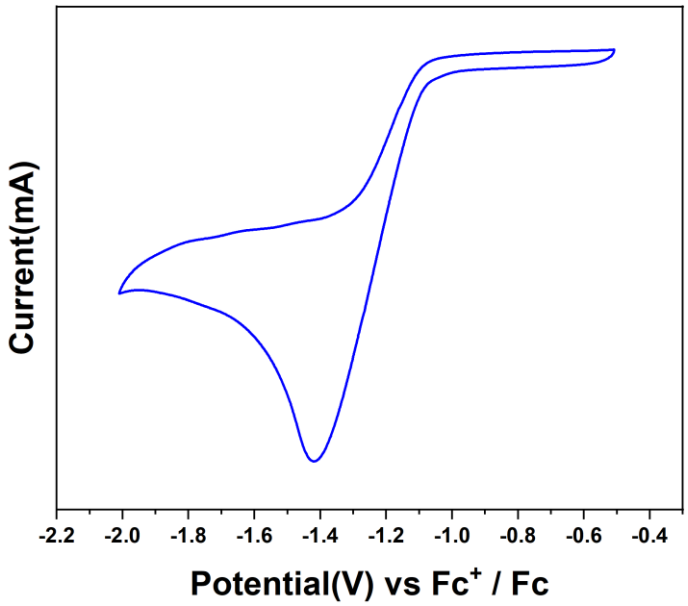

Figure S10. Cyclic voltammogram of **PerNN-MeI** in THF with 0.1 M Bu_4NPF_6 as a supporting electrolyte.

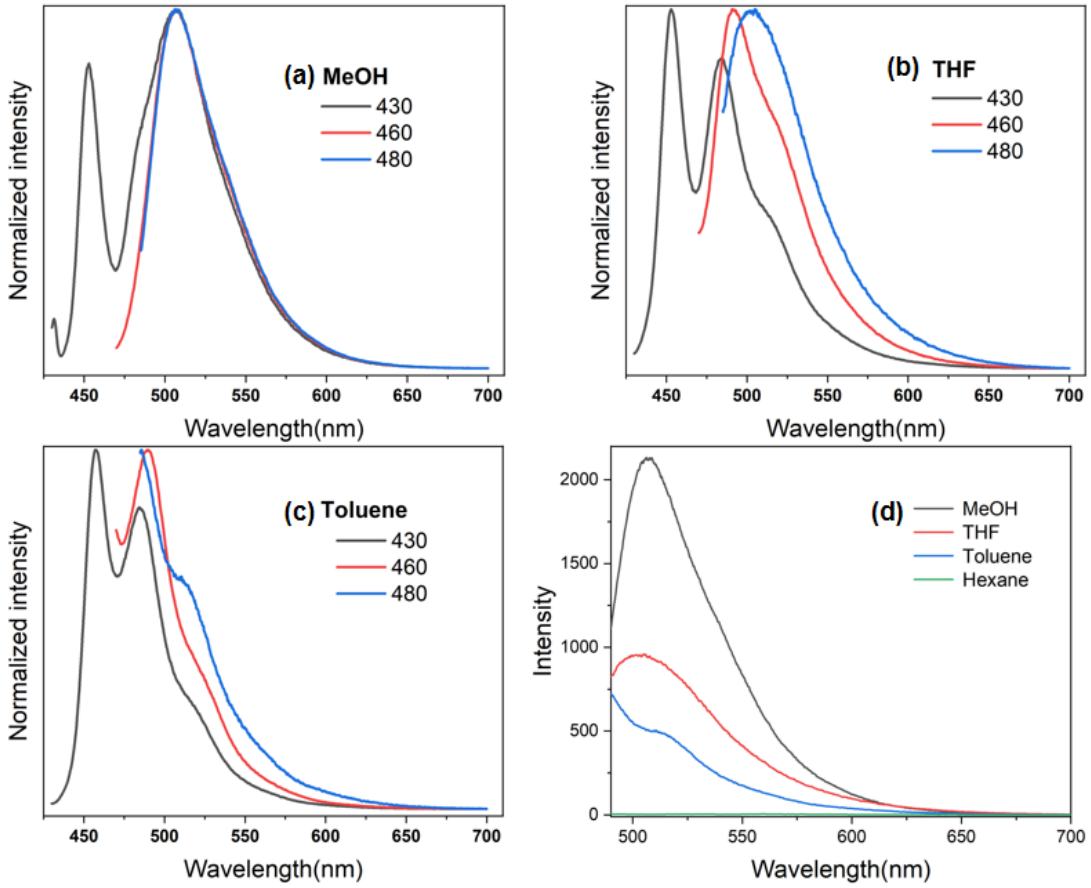

Figure S11. Excitation-dependant-emission spectra of **PerNN-MeI** in (a) MeOH (b) THF (c) Toluene; (d) Emission spectra of **PerNN-MeI** in four solvents when excited at 480 nm.

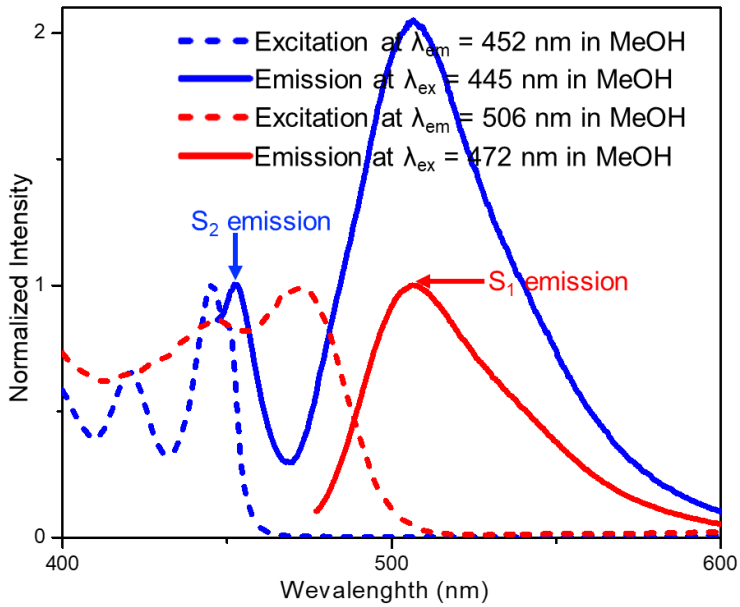

Figure S12. Excitation spectra (dotted line) and emission spectra (solid line) of **PerNN-MeI** in MeOH.

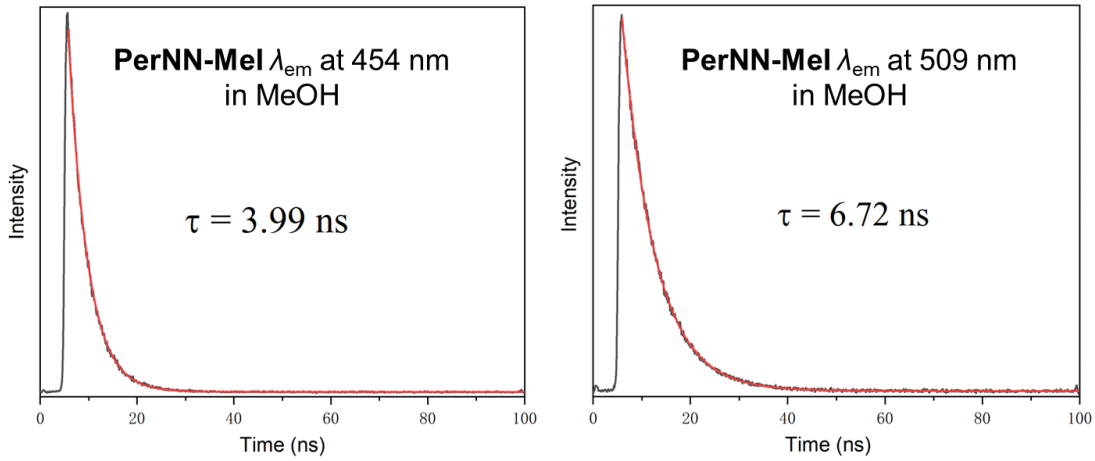

Figure S13. Fluorescence decay curves of **PerNN-MeI** recorded in MeOH solution, and their single-exponential fits. Experimental decay curves are shown in black, exponential fits are in red.

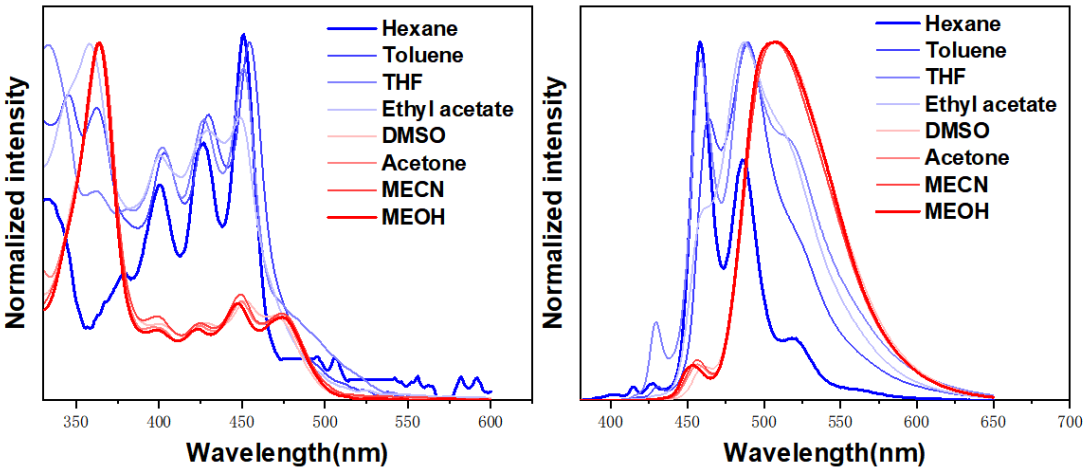

Figure S14. UV–vis absorption (left; 10^{-5} M) and emission (right; 10^{-5} M; excited with 370 nm) spectra of **PerNN-MeCl** in different solvents.

Table S5. Summarize the photophysical properties of **PerNN-MeCl** in different solvents.

Solvent	**Hexane**	**Toluene**	**THF**	**Ethyl acetate**	**DMSO**	**Acetone**	**MeCN**	**MeOH**
λ_{abs}/nm	451	455	451	448	469	472	474	474
λ_{em}/nm	459	490	488	488	509	507	507	507
QY(%)	55.00		39.78					35.10

Note: λ_{em} denotes the maximum emission wavelength.

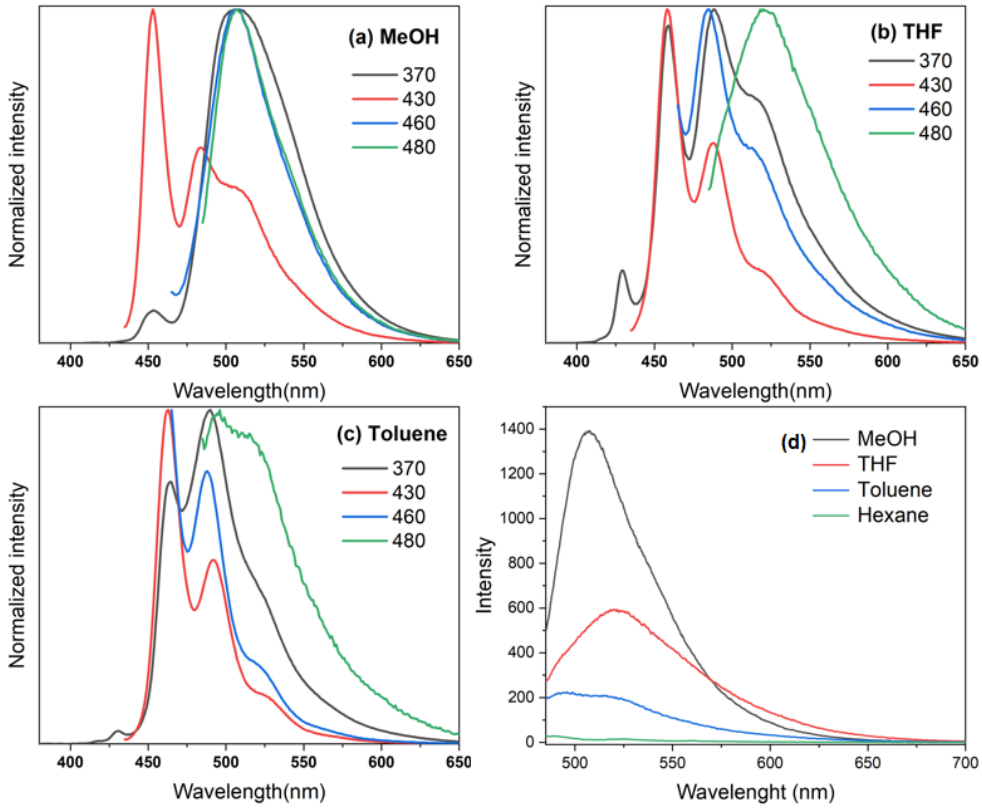

Figure S15. Excitation-dependant-emission spectra of **PerNN-MeCl** in (a) MeOH (b) THF (c) Toluene; (d) (d) Emission spectra of **PerNN-MeCl** in four solvents when excited at 480 nm.

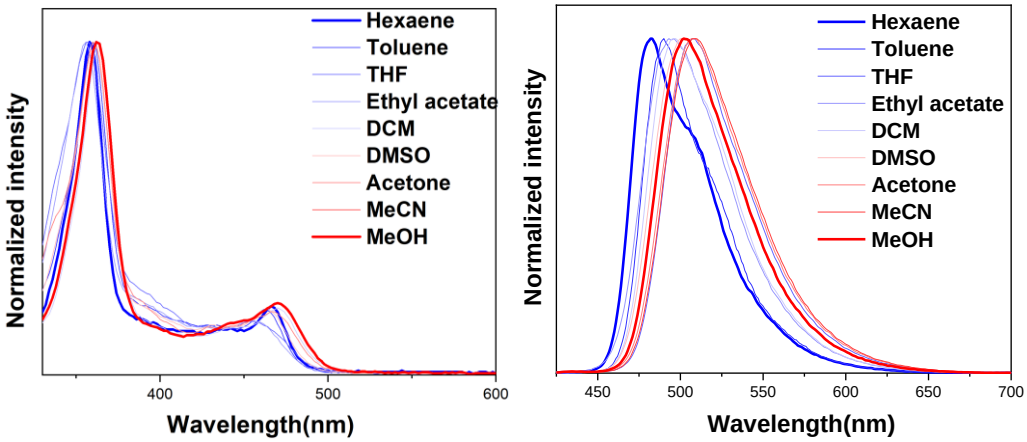

Figure S16. UV–vis absorption (left; 10^{-5} M) and emission (right; 10^{-5} M; excited with 420 nm) spectra of **PerNN-H** in different solvents.

Table S6. Summarize the photophysical properties of **PerNN-H** in different solvents.

Solvent	**Hexane**	**Toluene**	**THF**	**Ethyl acetate**	**DCM**	**DMSO**	**Acetone**	**MeCN**	**MeOH**	**Powder**
λ_{abs}/nm	465	462	455	453	469	463	467	469	467	
λ_{em}/nm	481	489	507	494	496	501	507	508	503	
QY(%)	33.23	38.93	33.06	32.29	23.90	36.56	35.17	33.78	38.20	4.40

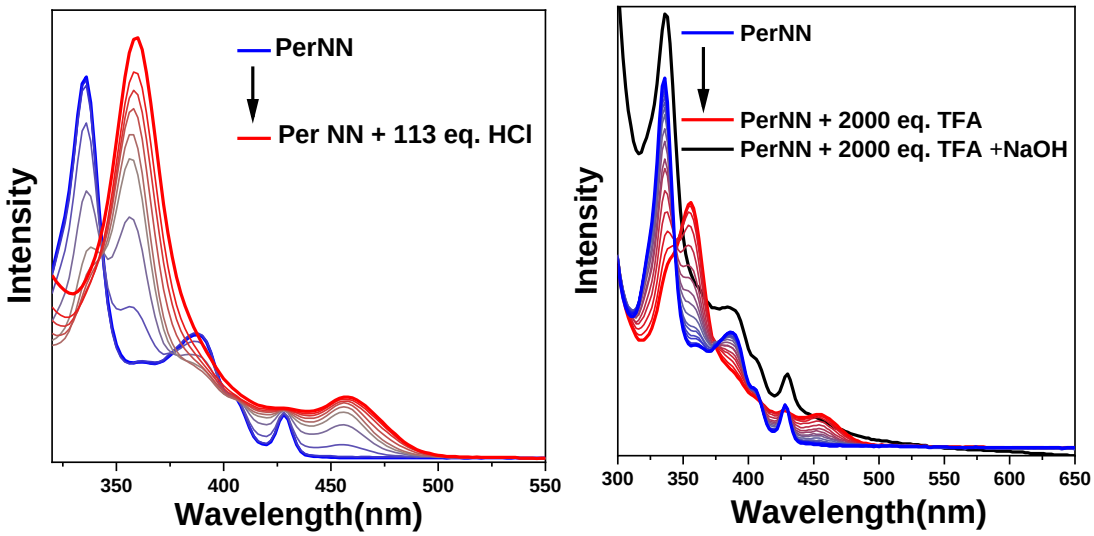

Figure S17. Acid (HCl, left; TFA, right)-induced UV-Vis absorption changes of compound **PerNN** in THF, and finally neutralized by NaOH (Concentration of **PerNN** is 10^{-5} M).

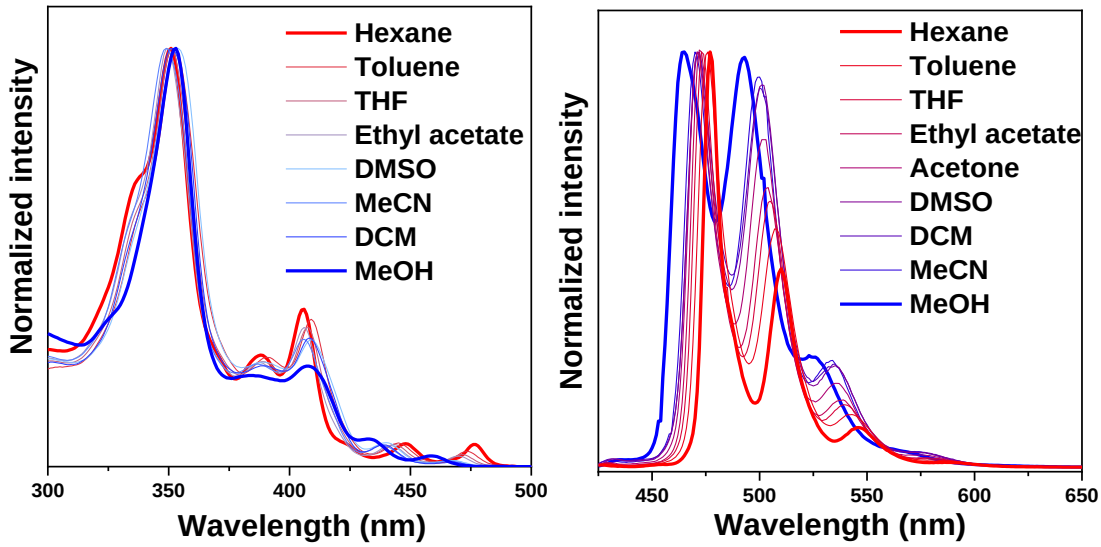

Figure S18. UV–vis absorption (left; 10^{-5} M) and emission (right; 10^{-5} M; excited with 370 nm) spectra of **PerNN-O** in different solvents.

Table S7. Summarize the photophysical properties of **PerNN-O** in different solvents.

Solvent	**Hexane**	**Toluene**	**THF**	**Ethyl acetate**	**DCM**	**DMSO**	**MeCN**	**MeOH**
λ_{abs}/nm	476	473	471	470	466	467	465	458
λ_{em}/nm	476	476	473	472	471	471	471	464
QY(%)			8.00					

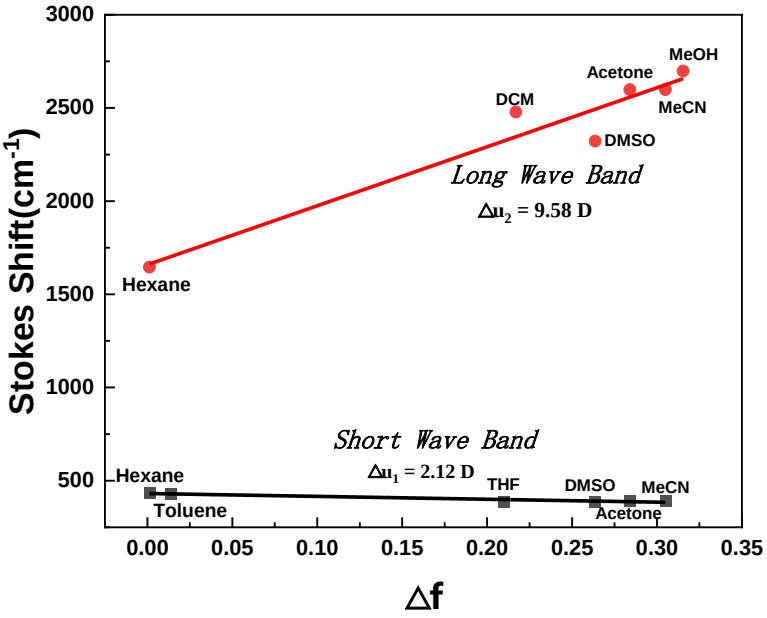

Figure S19. Lippert-Mataga solvatochromic model of **PerNN-MeI**.

4. DFT calculations

Theoretical calculations were performed using the Gaussian 16 software package and Multiwfn programm.[2] [3] [4] Unless stated otherwise, geometry optimizations of all molecules in the ground state (S_0) were performed using the B3LYP/6-31**. The simulated electronic absorption spectra are on the basis of the optimized ground-state geometry and wavefunction by time-dependent density functional theory (TD-DFT) calculation at B3LYP/6-311** level. The simulated electronic emission spectra are based on the optimized excited state geometries by TD-DFT calculation at B3LYP/6-311** level. Nucleus independent chemical shifts (NICS)[6] values and anisotropy of the induced current density (ACID)[7] plot for the simulated aromatic properties of studied molecules have been computed at the B3LYP/6-311** level based on the optimized ground-state geometries. Electrostatic potential (ESP) on the basis of the geometry and wavefunction at B3LYP/6-31** level were performed with the Multiwfn 3.8 (dev) code. Isosurface maps of various real space functions were rendered by means of Visual Molecular Dynamics (VMD) software based on the files exported by Multiwfn. [4] [5]

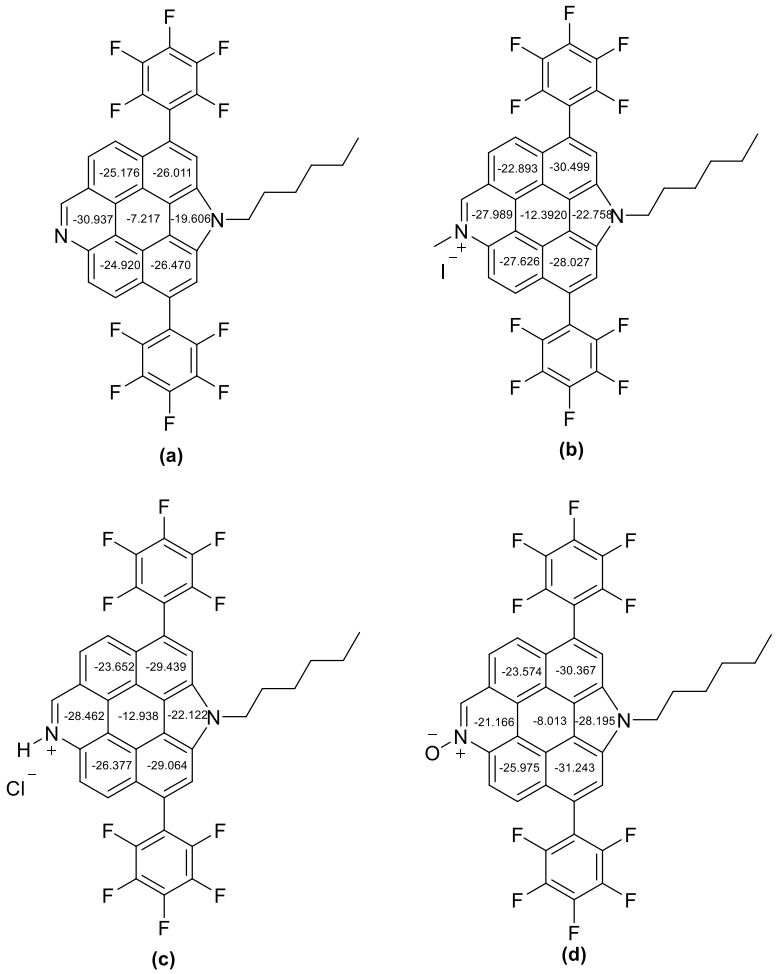

Figure S20. NICS(-1)$_{zz}$ plots of (a) **PerNN**, (b) **PerNN-Me$^+$**, (c) **PerNN-H** and (d) **PerNN-O** calculated at B3LYP/6-311G**. [6]

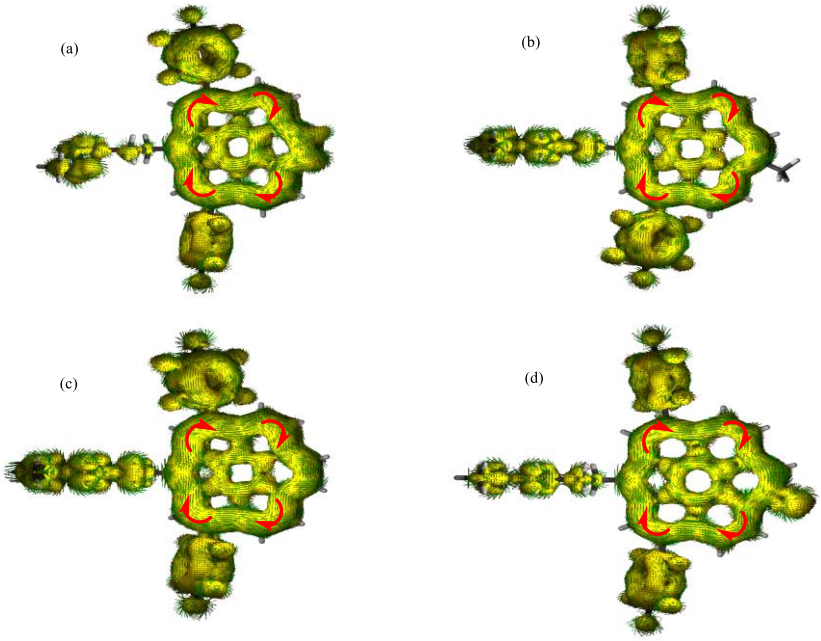

Figure S21. Calculated AICD plots (iso-value = 0.015- 0.03) of (a) **PerNN**, (b) **PerNN-Me$^+$**, (c) **PerNN-H** and (d) **PerNN-O**.

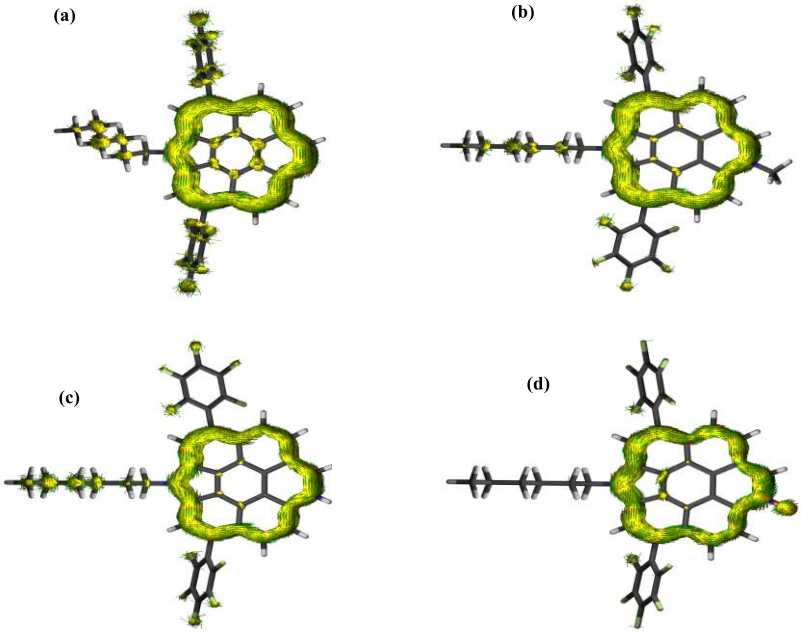

Figure S22. Calculated AICD plots (contribution from π electrons only, iso-value = 0.04 - 0.05) of (a) **PerNN**, (b) **PerNN-Me$^+$**, (c) **PerNN-H** and (d) **PerNN-O**. [7]

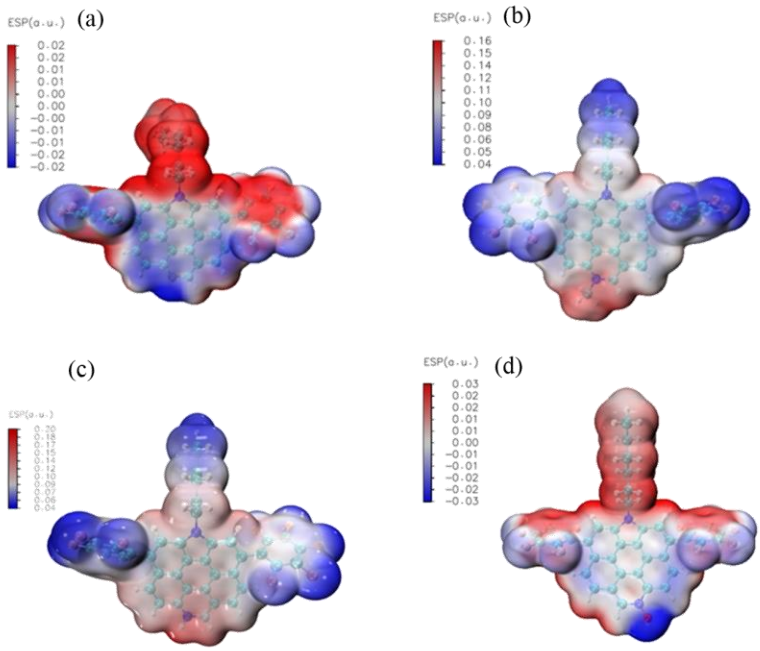

Figure S23. ESP plots of (a) **PerNN**, (b) **PerNN-Me$^+$**, (c) **PerNN-H** and (d) **PerNN-O** calculated at B3LYP/6-31G**. [4] [5]

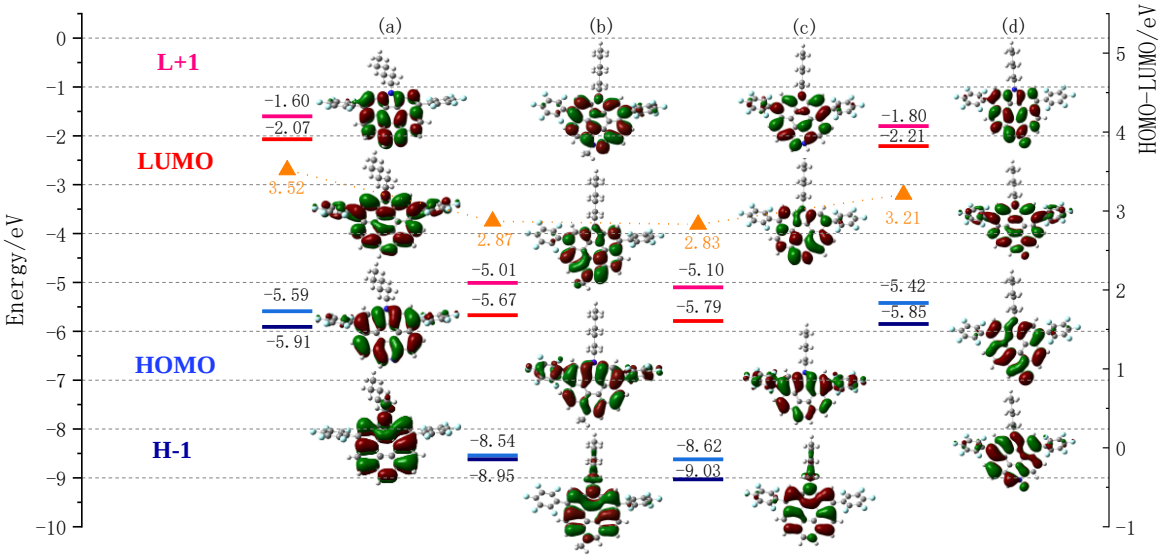

Figure S24. HOMO-1, HOMO, LUMO and LUMO+1 orbitals and their energy levels of (a) **PerNN**, (b) **PerNN-Me$^+$**, (c) **PerNN-H** and (d) **PerNN-O** calculated at B3LYP/6-31G**.

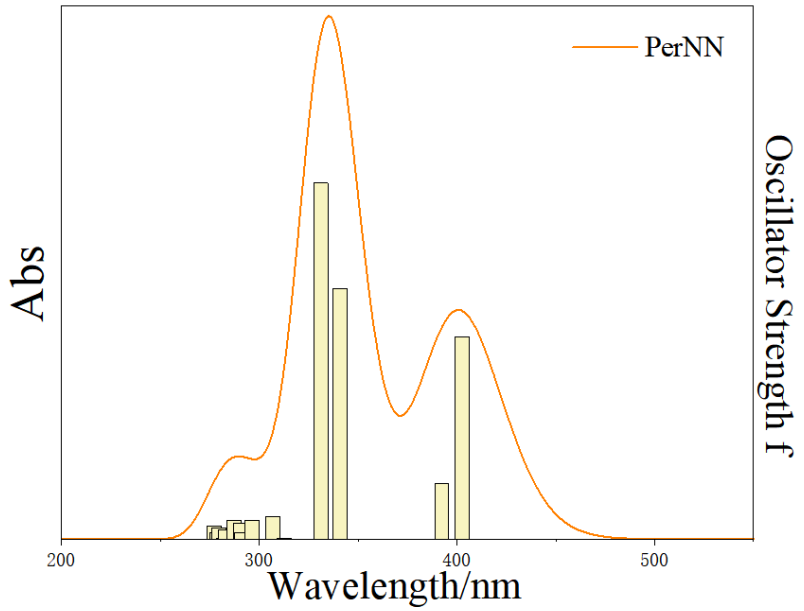

Figure S25. TD-DFT (B3LYP/6-311G**) simulated UV-Vis-NIR absorption spectra with oscillator strength of compound **PerNN**.

Table S8. Selected TD-DFT (B3LYP/6-311G**) calculated absorption wavelength, oscillator strength and compositions of major electronic transitions of **PerNN**.

	State	Energy [eV]	λ [nm]	*f*	Orbitals(coefficient)
PerNN	S1	3.08	403	0.3792	HOMO→LUMO (78%)
	S2	3.17	392	0.1044	H-1→LUMO (55%), HOMO→LUMO (12%), HOMO→L+1 (31%)
	S3	3.64	341	0.4694	H-1→LUMO (32%), HOMO→L+1 (54%)
	S4	3.75	331	0.6672	H-1→L+1 (80%)
	S5	3.97	312	0.0021	HOMO→L+3 (85%)
	S6	4.05	307	0.0424	HOMO→L+2 (95%)
	S7	4.19	296	0.0359	H-2→LUMO (79%)
	S8	4.26	291	0.013	H-6→LUMO (48%), H-1→L+3 (25%)
	S9	4.27	291	0.03	H-6→LUMO (30%), H-1→L+3 (50%)
	S10	4.33	287	0.0359	H-2→LUMO (11%), H-1→L+2 (60%)
	S11	4.39	283	0.0178	H-3→LUMO (27%), H-1→L+2 (24%), HOMO→L+4 (15%), HOMO→L+6 (11%)
	S12	4.40	282	0.0016	H-6→LUMO (14%), H-6→L+1 (75%)
	S13	4.44	280	0.0215	H-4→LUMO (34%), H-3→LUMO (22%), HOMO→L+4 (21%), HOMO→L+5 (10%)

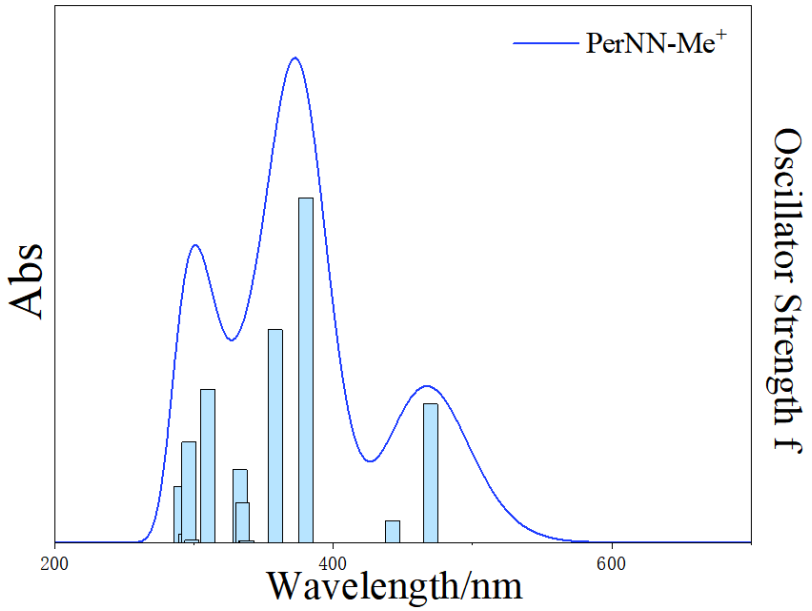

Figure S26. TD-DFT (B3LYP/6-311G**) simulated UV-Vis-NIR absorption spectra with oscillator strength of compound **PerNN-Me**$^+$.

Table S9. Selected TD-DFT (B3LYP/6-311G**) calculated absorption wavelength, oscillator strength and compositions of major electronic transitions of **PerNN-Me**$^+$.

	State	Energy [eV]	λ [nm]	*f*	Orbitals(coefficient)
PerNN-Me$^+$	S1	2.64	470	0.2195	HOMO→LUMO (93%)
	S2	2.81	443	0.0346	H-1→LUMO (80%), HOMO→L+1 (17%)
	S3	3.27	380	0.5457	H-1→LUMO (12%), HOMO→L+1 (73%)
	S4	3.47	358	0.3369	H-1→L+1 (85%)
	S5	3.68	338	0.0032	H-3→LUMO (64%), H-2→LUMO (29%)
	S6	3.68	338	0.0034	H-3→LUMO (31%), H-2→LUMO (67%)
	S7	3.71	335	0.0623	H-5→LUMO (19%), H-4→LUMO (72%)
	S8	3.73	333	0.1157	H-5→LUMO (67%), H-4→LUMO (20%)
	S9	4.01	310	0.2427	HOMO→L+2 (90%)
	S10	4.16	299	0.0041	H-2→L+1 (96%)
	S11	4.19	297	0.1595	H-7→LUMO (14%), H-5→L+1 (26%), H-4→L+1 (33%)
	S13	4.22	294	0.0126	H-3→L+1 (88%)
	S14	4.27	291	0.0892	H-6→LUMO (12%), H-5→L+1 (39%), H-4→L+1 (22%), HOMO→L+3 (12%)
	S15	4.27	291	0.0701	H-7→LUMO (40%), H-4→L+1 (25%), HOMO→L+3 (18%)

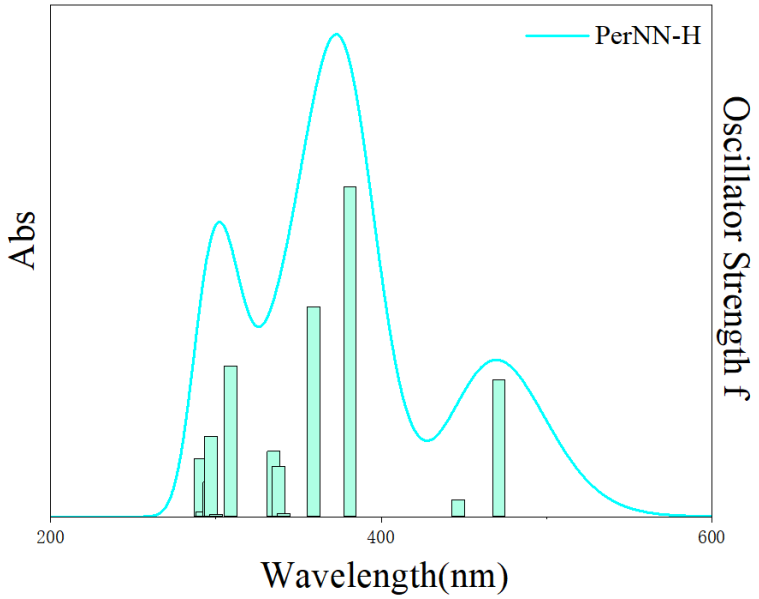

Figure S27. TD-DFT (B3LYP/6-311G**) simulated UV-Vis-NIR absorption spectra with oscillator strength of compound **PerNN-H**.

Table S10. Selected TD-DFT (B3LYP/6-311G**) calculated absorption wavelength, oscillator strength and compositions of major electronic transitions of **PerNN-H**.

	State	Energy [eV]	λ [nm]	*f*	Orbitals(coefficient)
PerNN-H	S1	2.64	471	0.2143	HOMO→LUMO (93%)
	S2	2.78	447	0.0266	H-1→LUMO (82%), HOMO→L+1 (15%)
	S3	3.26	381	0.5153	H-1→LUMO (11%), HOMO→L+1 (75%)
	S4	3.46	359	0.3287	H-1→L+1 (85%)
	S6	3.64	341	0.0050	H-3→LUMO (80%), H-2→LUMO (18%)
	S7	3.67	338	0.0792	H-5→LUMO (13%), H-4→LUMO (80%)
	S8	3.71	335	0.1025	H-5→LUMO (76%), H-4→LUMO (12%)
	S9	4.02	309	0.2355	HOMO→L+2 (89%)
	S10	4.14	300	0.0035	H-2→L+1 (97%)
	S11	4.18	297	0.1258	H-7→LUMO (10%), H-5→L+1 (18%), H-4 →L+1 (23%), H-3→L+1 (34%)
	S12	4.19	296	0.0541	H-6→LUMO (10%), H-4→L+1 (10%), H-3 →L+1 (60%)
	S13	4.20	296	0.0079	H-6→LUMO (61%), H-4→L+1 (15%)
	S14	4.25	292	0.0076	H-5→L+1 (39%), H-4→L+1 (41%)

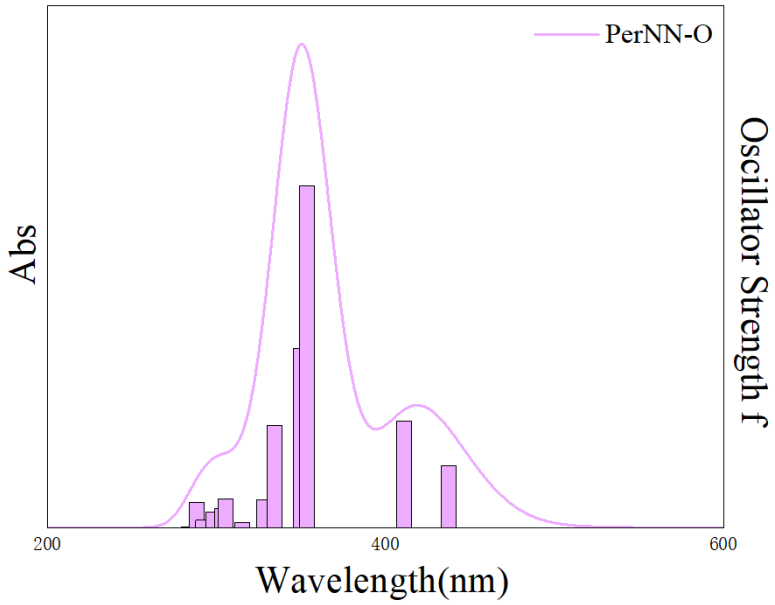

Figure S28. TD-DFT (B3LYP/6-311G**) simulated UV-Vis-NIR absorption spectra with oscillator strength of compound **PerNN-O**.

Table S11. Selected TD-DFT (B3LYP/6-311G**) calculated absorption wavelength, oscillator strength and compositions of major electronic transitions of **PerNN-O**.

	State	Energy [eV]	λ [nm]	*f*	Orbitals(coefficient)
PerNN-O	S1	2.84	437	0.1367	H-1→LUMO (14%), HOMO→LUMO (58%), HOMO→L+1 (20%)
	S2	3.02	411	0.2345	H-1→LUMO (44%), HOMO→LUMO (31%), HOMO→L+1 (21%)
	S3	3.51	354	0.7529	H-2→LUMO (14%), H-1→LUMO (30%), HOMO→L+1 (41%)
	S4	3.55	350	0.3948	H-1→L+1 (70%)
	S5	3.71	334	0.2258	H-2→LUMO (53%), HOMO→L+2 (25%)
	S6	3.79	328	0.0609	H-2→LUMO (19%), HOMO→L+2 (66%)
	S8	3.94	315	0.0100	HOMO→L+3 (86%)
	S9	4.07	305	0.0616	H-2→L+1 (39%), H-1→L+2 (45%)
	S10	4.10	303	0.0409	H-2→L+1 (38%), H-1→L+2 (44%)
	S11	4.17	298	0.0349	H-4→LUMO (42%), H-3→LUMO (12%), H-1→L+3 (29%)
	S12	4.25	292	0.0157	H-4→LUMO (26%), H-1→L+3 (54%)
	S14	4.31	288	0.0550	H-1→L+3 (11%), HOMO→L+4 (45%), HOMO→L+6 (22%)
	S15	4.38	284	0.0020	H-6→LUMO (60%), H-5→LUMO (11%), HOMO→L+5 (14%)

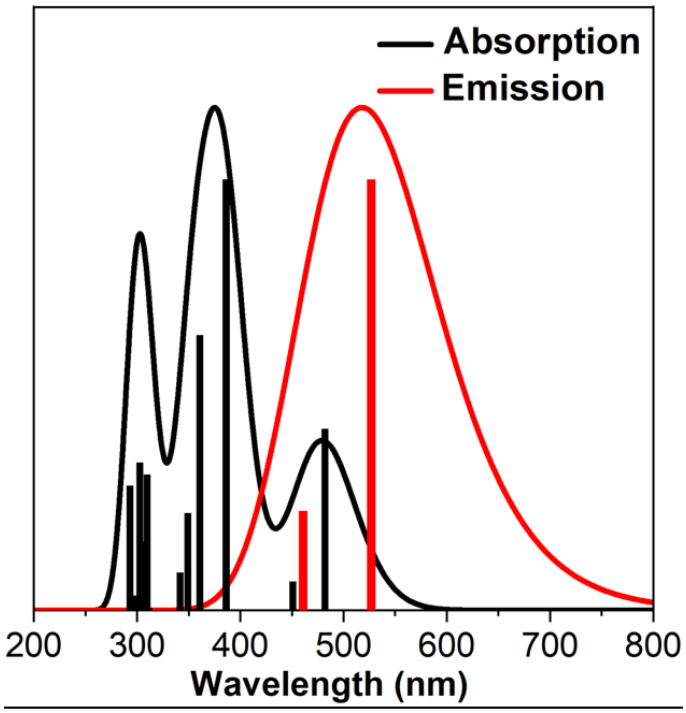

State	Energy [eV]	λ [nm]	f
S1	2.36	527	0.2007
S2	2.69	461	0.0463

Figure S29. Simulated absorption and emission spectra, and vertical $S_n \rightarrow S_0$ deexcitation, oscillation strengths (f) of **PerNN-Me**$^+$ based on the optimized ground state (absorption) and optimized excited state (emission) geometry calculated at the B3LYP/6-311** level.

Crystal information

Single crystal **PerNN** is obtained by slow diffusion of hexane to a solution of **PerNN** in chloroform at room temperature over five days.

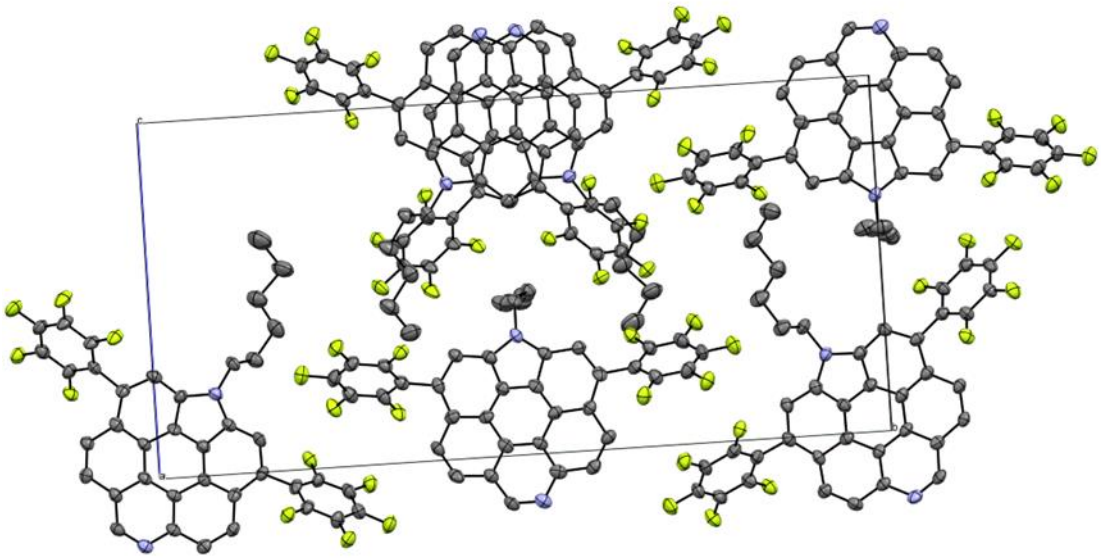

Figure S30. Packing mode of single crystal **PerNN** in a unit cell viewed along a axis.

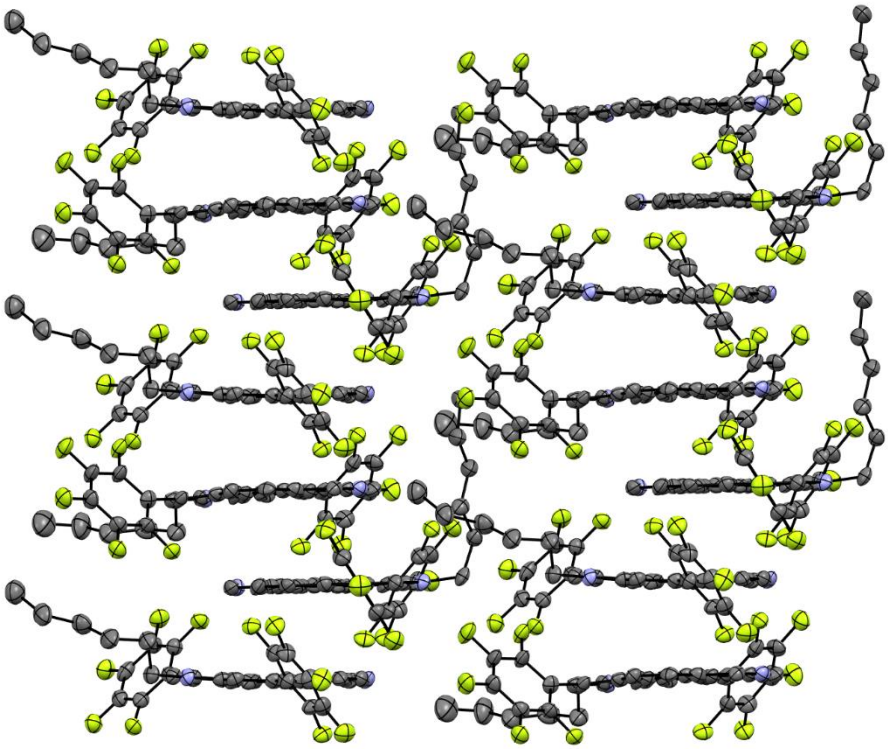

Figure S31. Packing mode of single crystal **PerNN**.

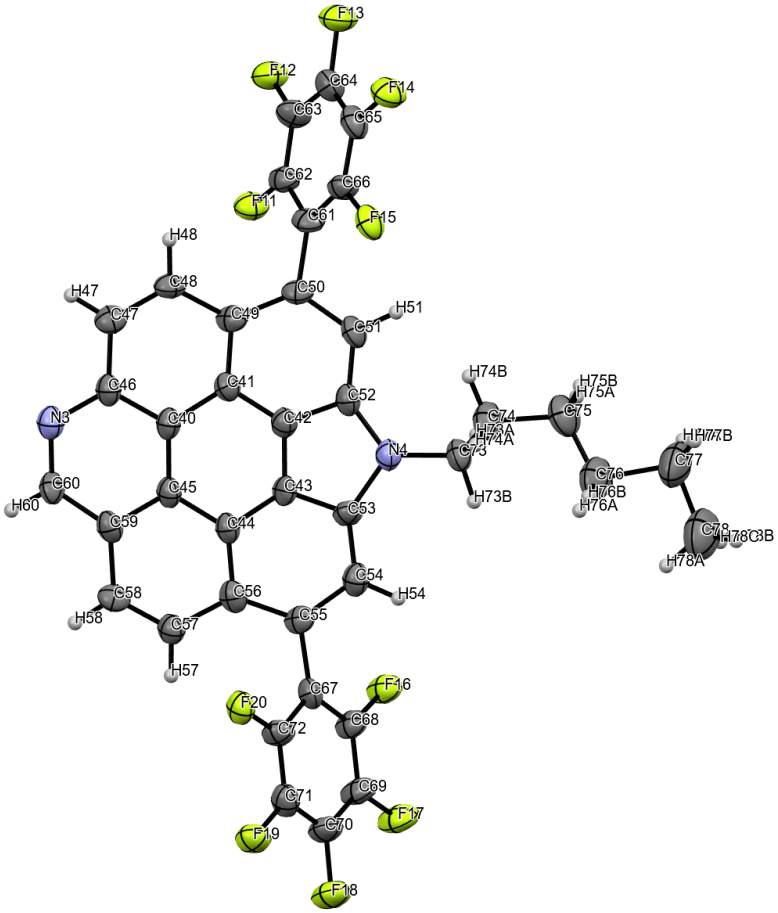

Figure S32. Thermal ellipsoid plot of **PerNN**.

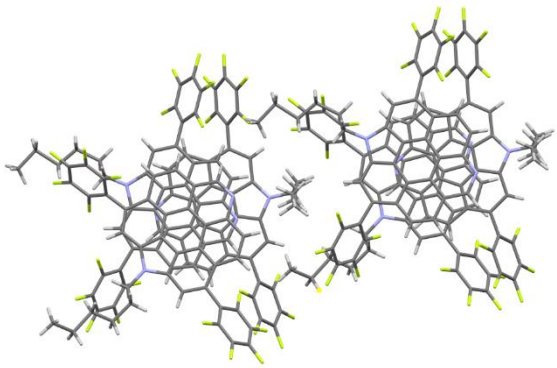

Figure S33. Top view of **PerNN** along a axis.

Table S12. Crystallographic data for **PerNN**.

Identification code	230425
Empirical formula	$C_{39}H_{20}N_2F_{10}$
Formula weight	706.57
Temperature/K	193.0

Crystal system	monoclinic
Space group	$P2_1$
a/Å	10.3159(5)
b/Å	30.2698(11)
c/Å	15.1352(6)
α/°	90
β/°	103.948(3)
γ/°	90
Volume/Å^3	4586.8(3)
Z	6
ρ_{calc}g/cm^3	1.535
μ/mm^{-1}	0.737
F(000)	2148.0
Crystal size/mm^3	0.18 × 0.18 × 0.02
Radiation	GaKα (λ = 1.34139)
2Θ range for data collection/°	5.08 to 111.996
Index ranges	$-12 \leq h \leq 12$, $-37 \leq k \leq 21$, $-18 \leq l \leq 17$
Reflections collected	28223
Independent reflections	13636 [R_{int} = 0.0517, R_{sigma} = 0.0519]
Data/restraints/parameters	13636/1/1381
Goodness-of-fit on F^2	1.054
Final R indexes [I>=2σ (I)]	R_1 = 0.0486, wR_2 = 0.1133
Final R indexes [all data]	R_1 = 0.0699, wR_2 = 0.1224
Largest diff. peak/hole / e Å^{-3}	0.49/-0.27
Flack parameter	0.09(10)

6. Appendix: $^{1}H/^{13}C$ NMR , HRMS spectra and IR spectra

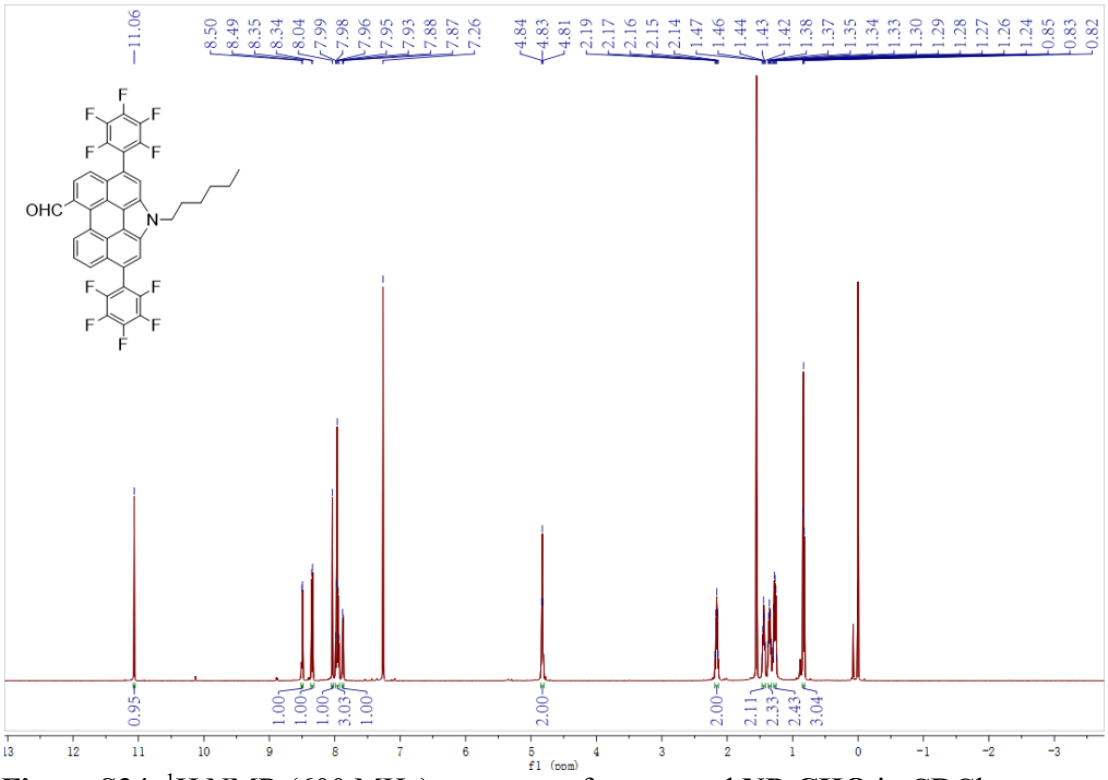

Figure S34. ^{1}H NMR (600 MHz) spectrum of compound **NP-CHO** in $CDCl_3$.

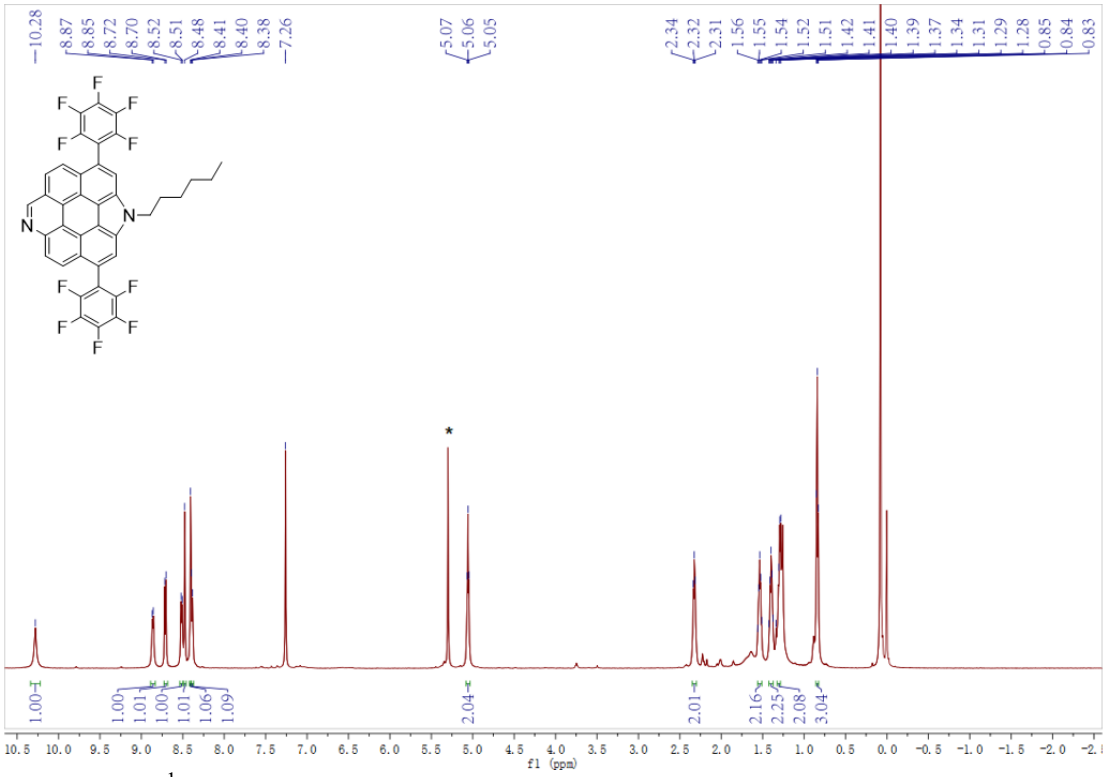

Figure S35. ^{1}H NMR (600 MHz) spectrum of compound **PerNN** in $CDCl_3$ (* denotes the impurity from solvent).

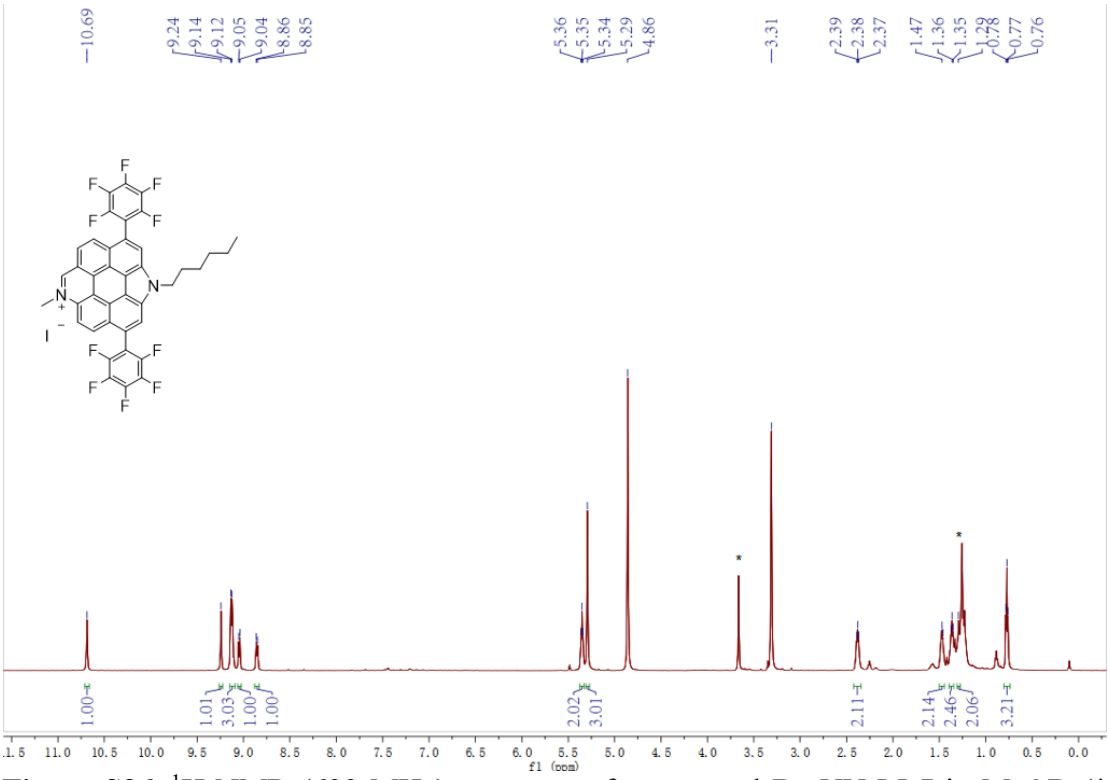

Figure S36. ^{1}H NMR (600 MHz) spectrum of compound **PerNN-MeI** in MeOD (* denotes the impurity from solvent).

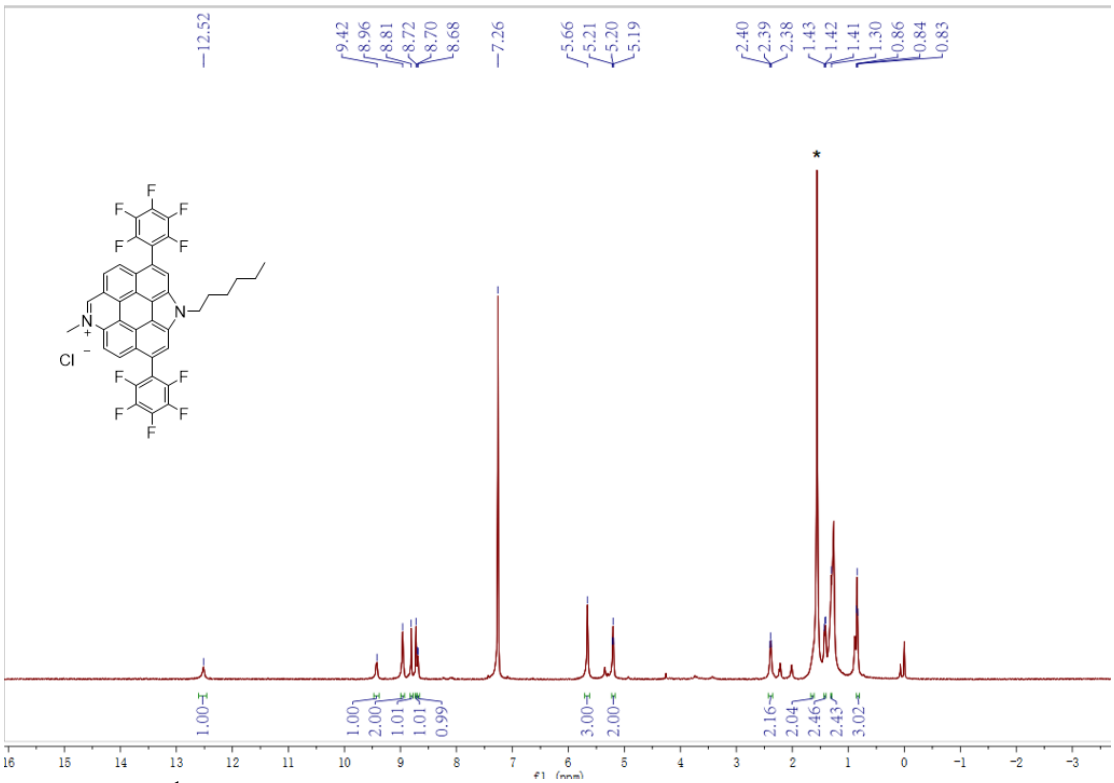

Figure S37. ^{1}H NMR (600 MHz) spectrum of compound **PerNN-MeCl** in $CDCl_3$ (* denotes the impurity from solvent).

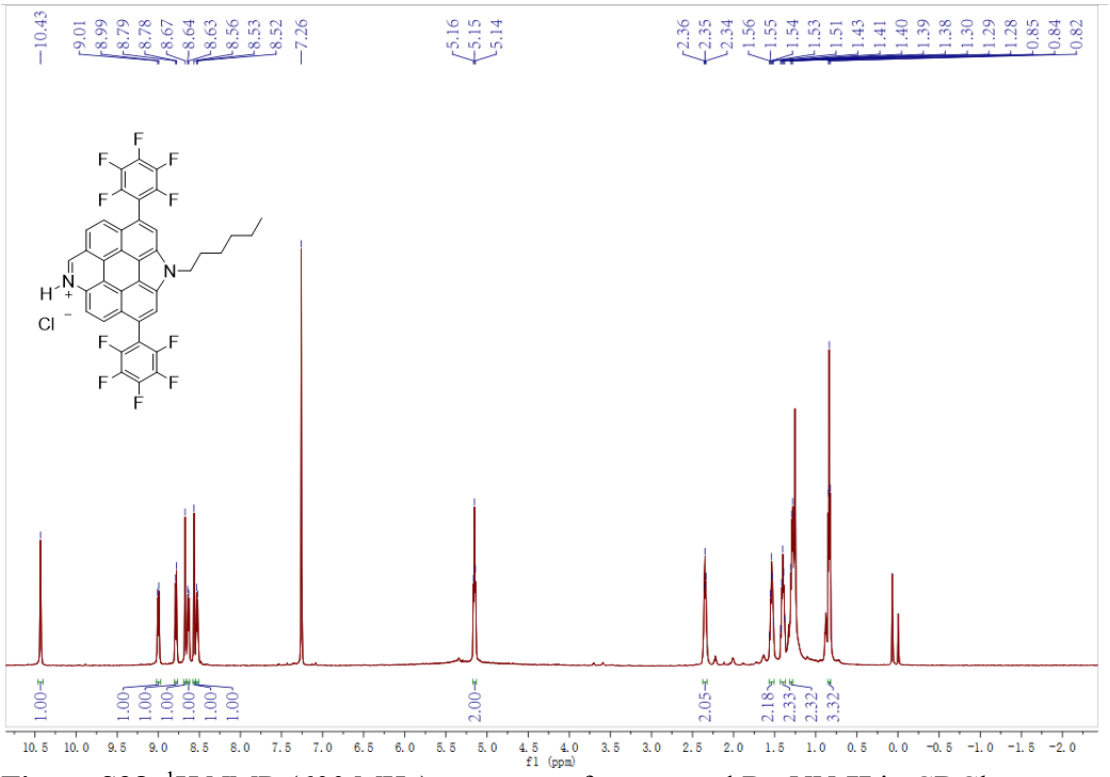

Figure S38. ^{1}H NMR (600 MHz) spectrum of compound **PerNN-H** in $CDCl_3$.

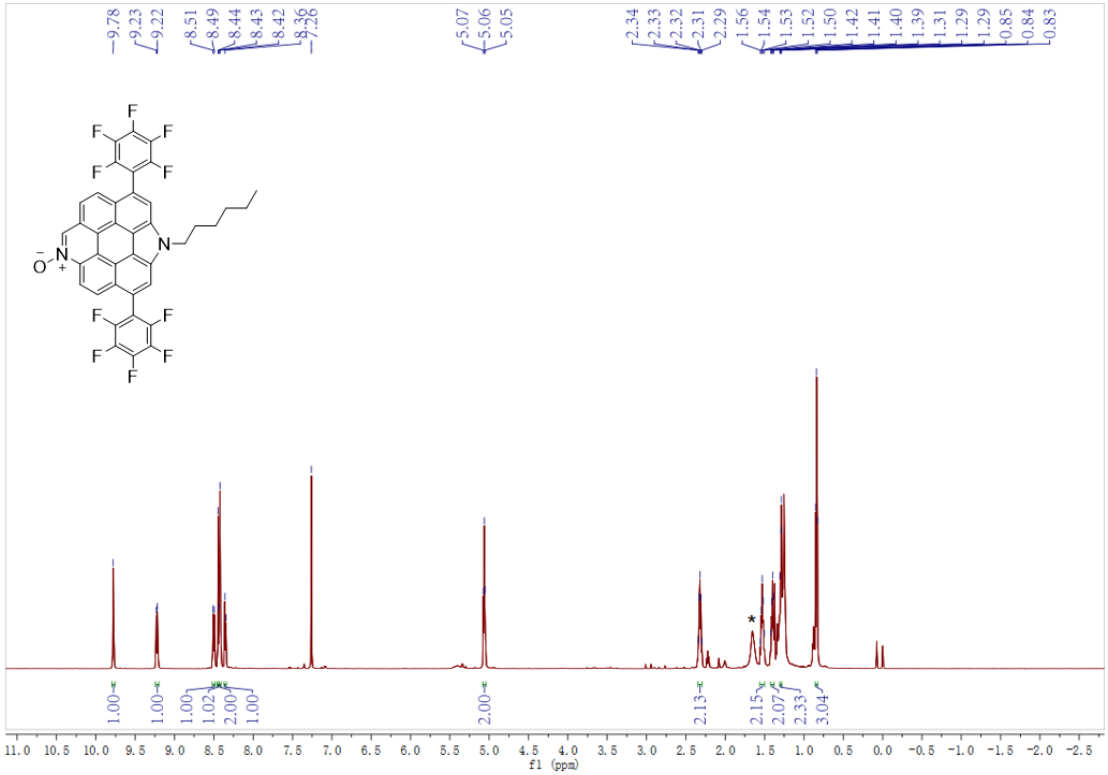

Figure S39. ^{1}H NMR (600 MHz) spectrum of compound **PerNN-O** in $CDCl_3$ (* denotes the impurity from solvent).

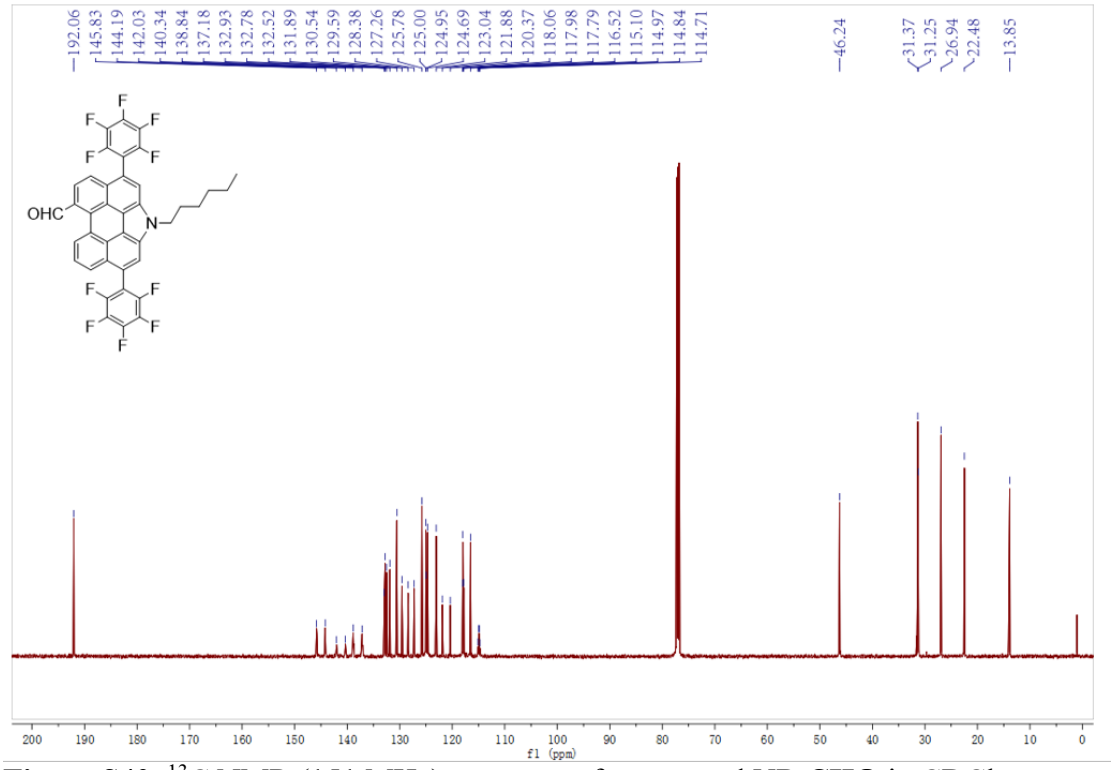

Figure S40. ^{13}C NMR (151 MHz) spectrum of compound **NP-CHO** in $CDCl_3$.

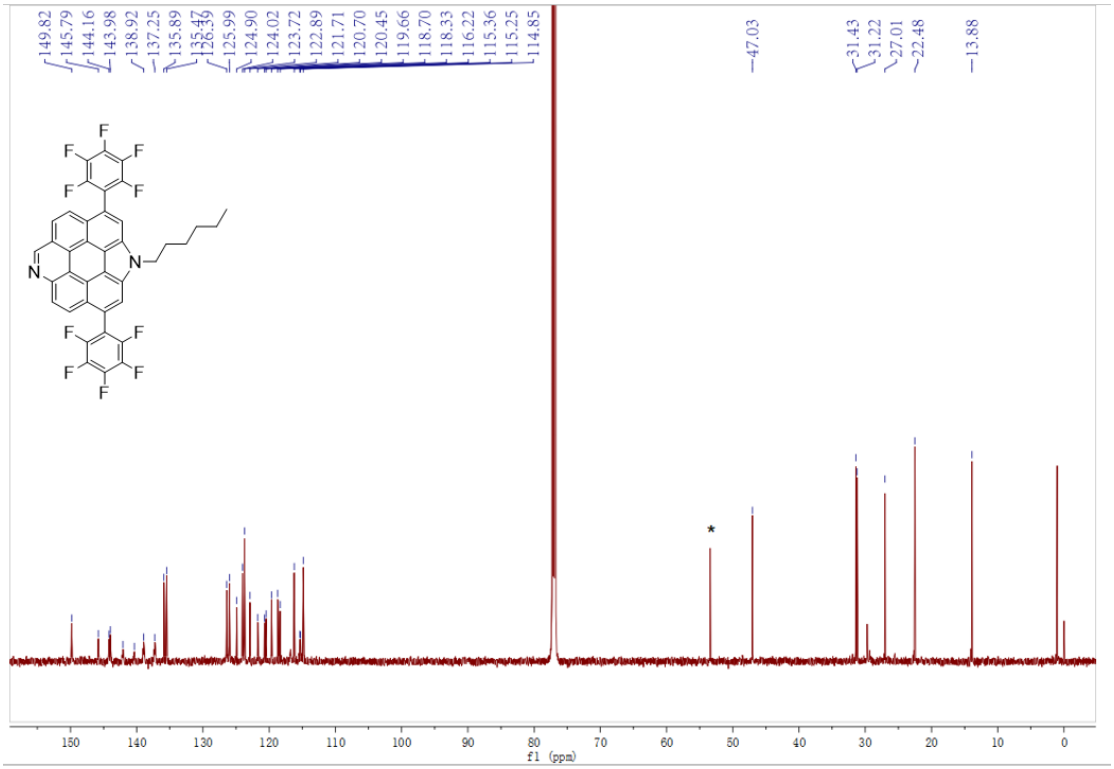

Figure S41. ^{13}C NMR (151 MHz) spectrum of compound **PerNN** in $CDCl_3$ (* denotes the impurity from solvent).

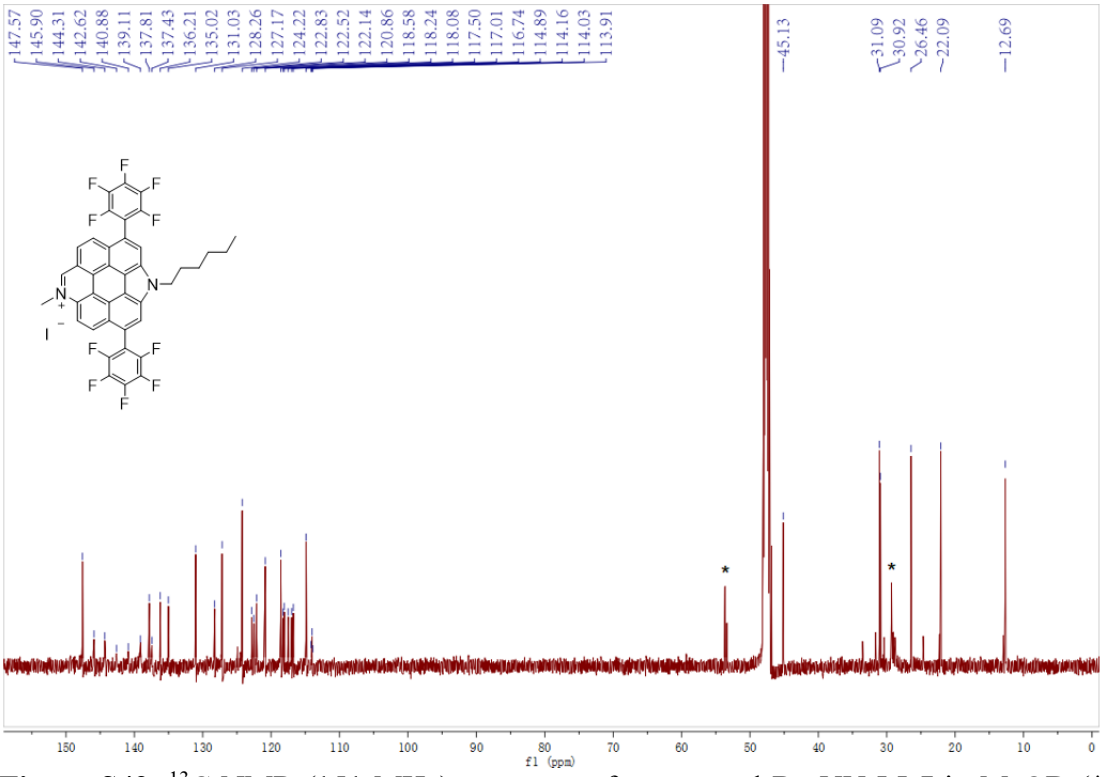

Figure S42. ^{13}C NMR (151 MHz) spectrum of compound **PerNN-MeI** in MeOD (* denotes the impurity from solvent).

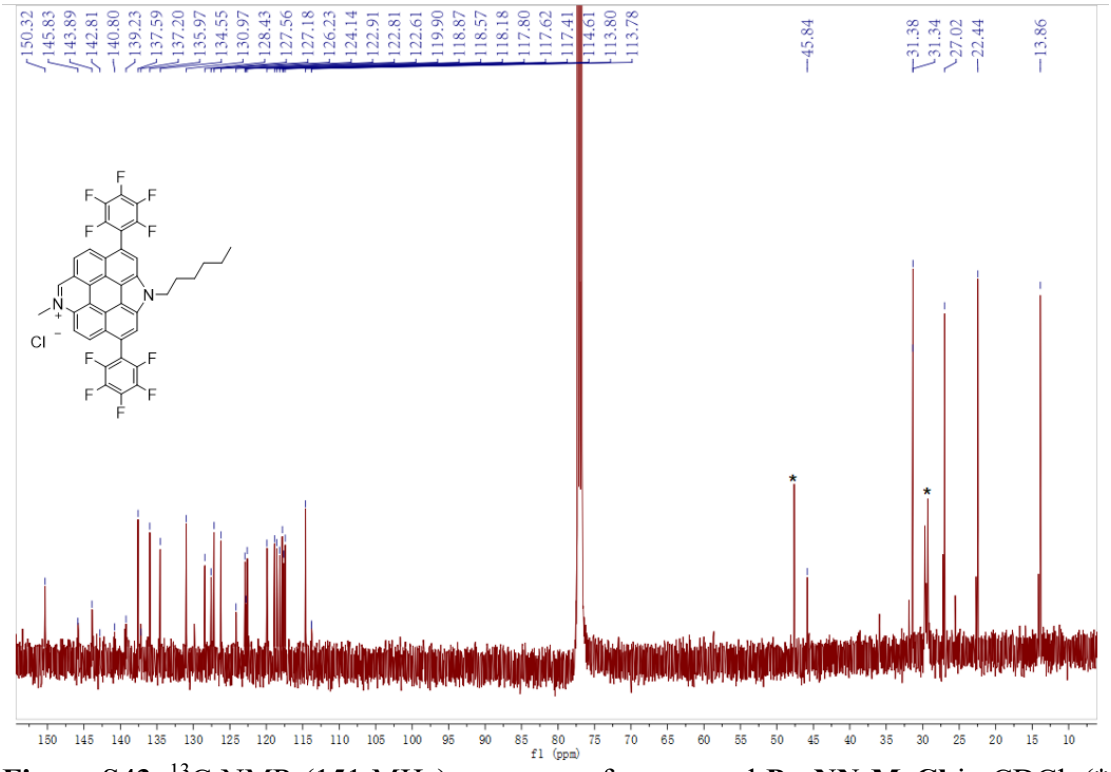

Figure S43. ^{13}C NMR (151 MHz) spectrum of compound **PerNN-MeCl** in $CDCl_3$ (* denotes the impurity from solvent).

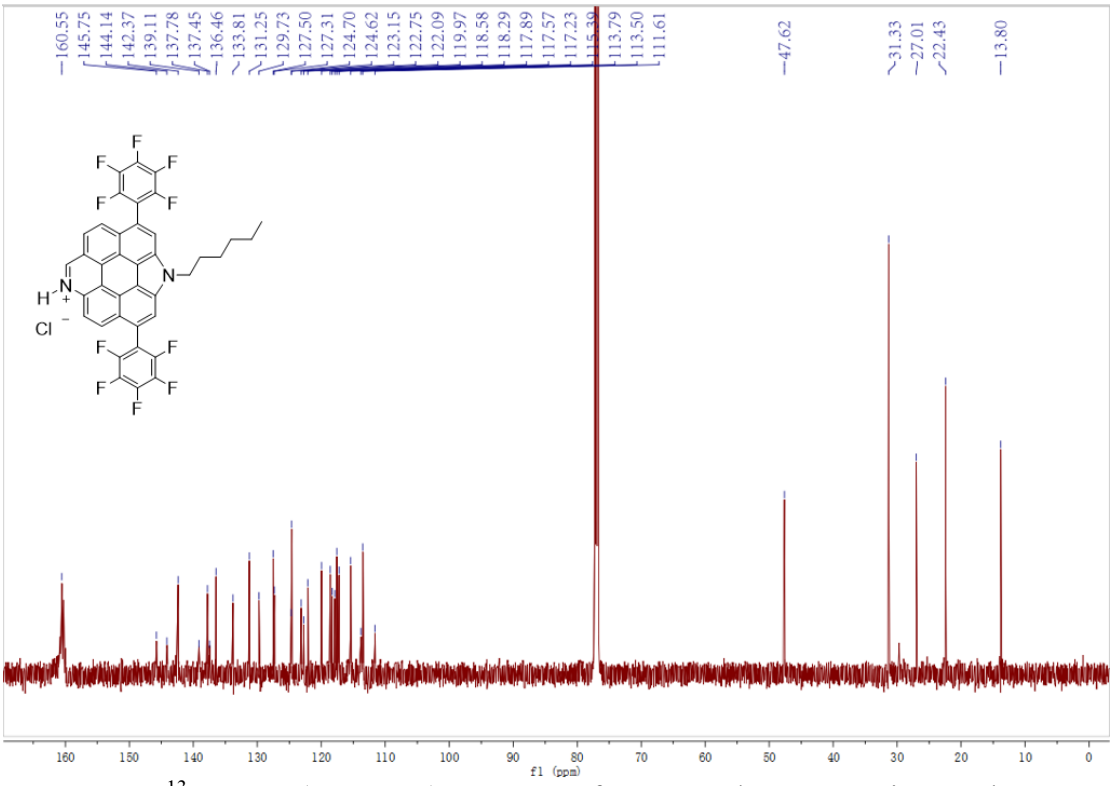

Figure S44. ^{13}C NMR (151 MHz) spectrum of compound **PerNN-H** in $CDCl_3$.

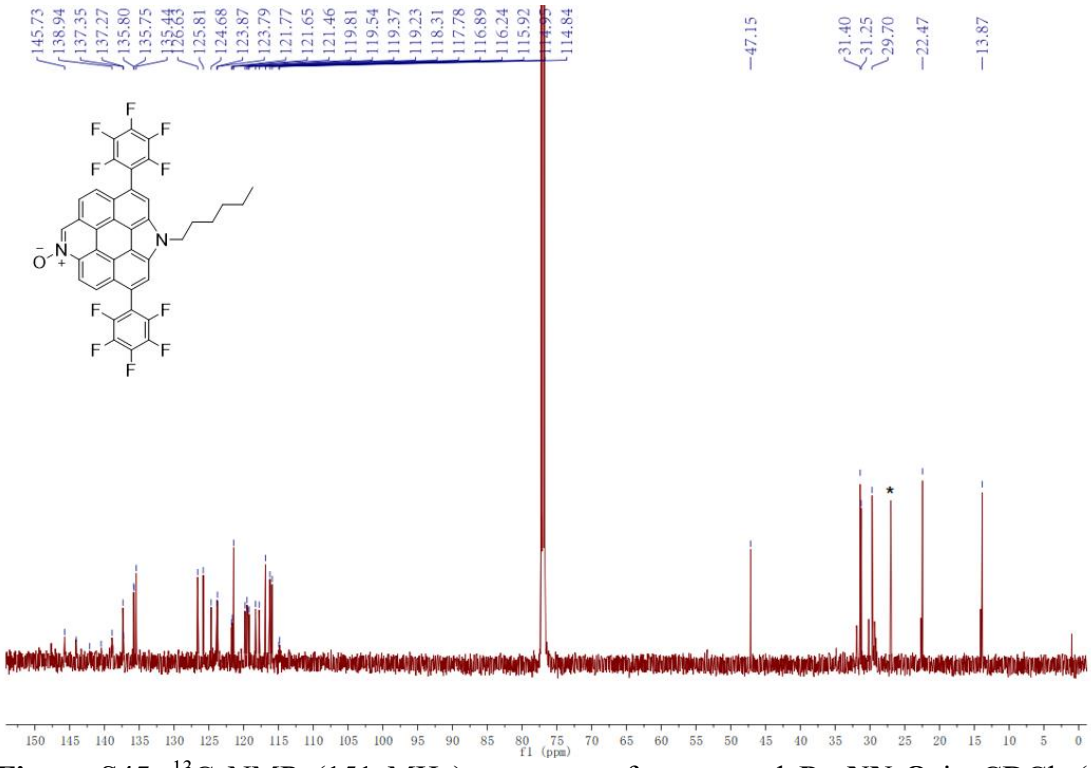

Figure S45. ^{13}C NMR (151 MHz) spectrum of compound **PerNN-O** in $CDCl_3$ (* denotes the impurity from solvent).

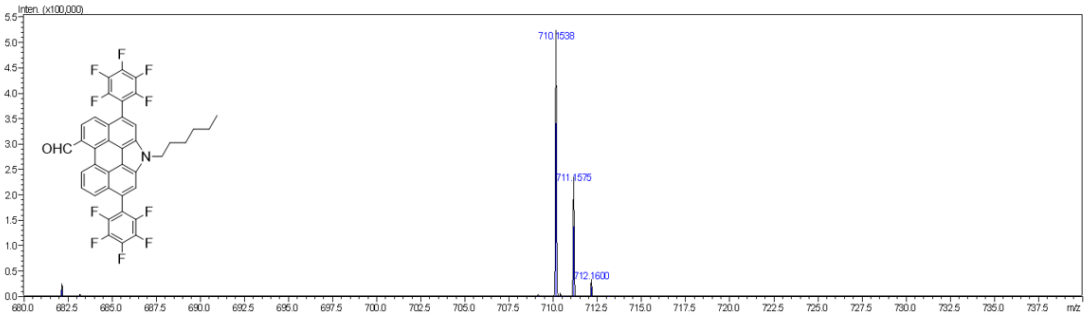

Figure S46. HRMS of compound **NP-CHO**.

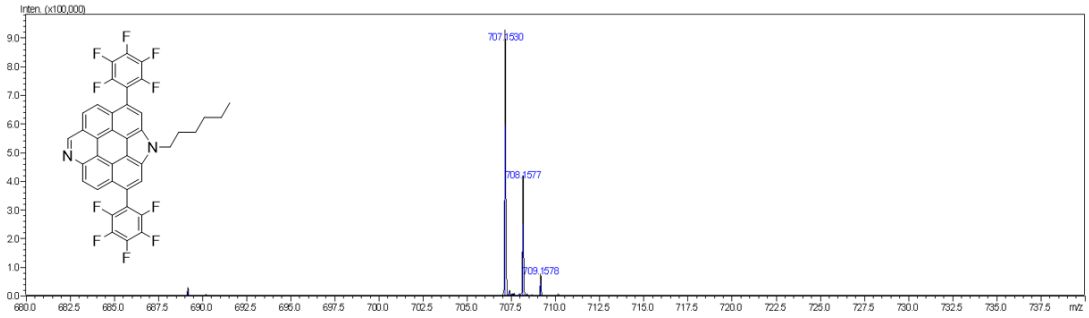

Figure S47. HRMS of compound **PerNN**.

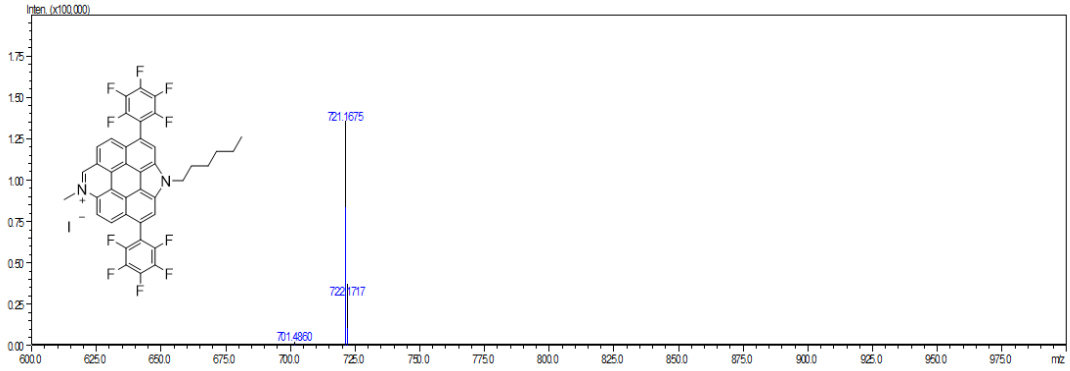

Figure S48. HRMS of compound **PerNN-MeI**.

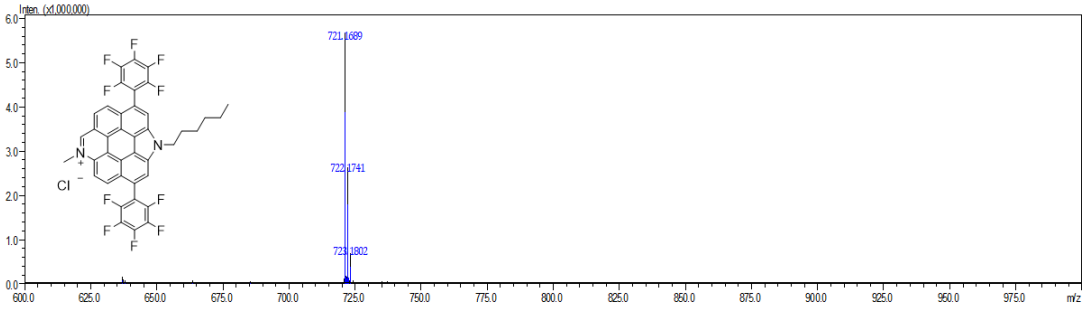

Figure S49. HRMS of compound **PerNN-MeCl**.

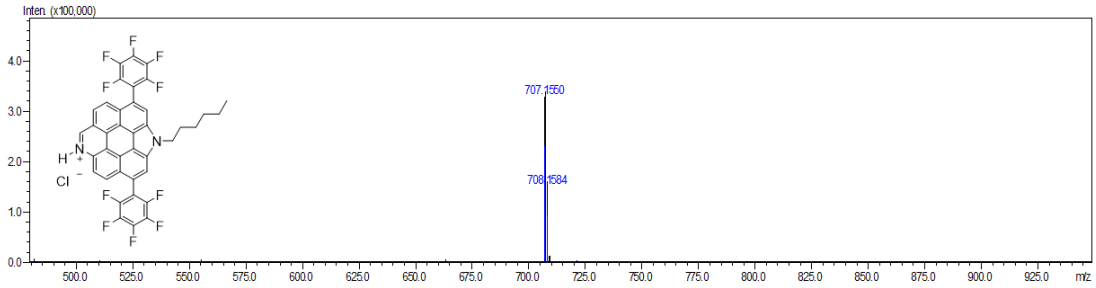

Figure S50. HRMS of compound **PerNN-H**.

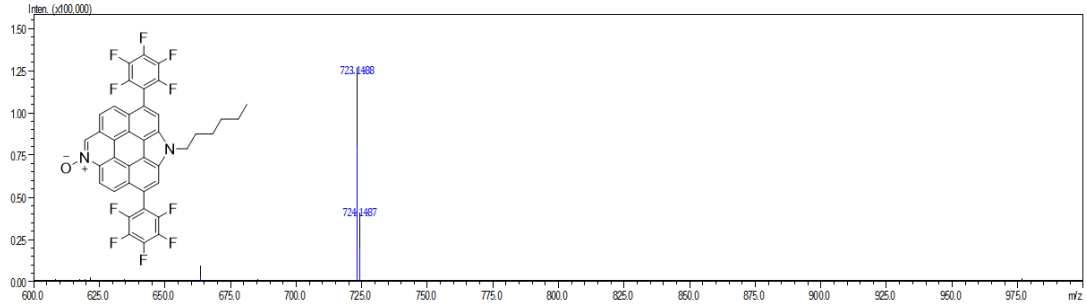

Figure S51. HRMS of compound **PerNN-O**.

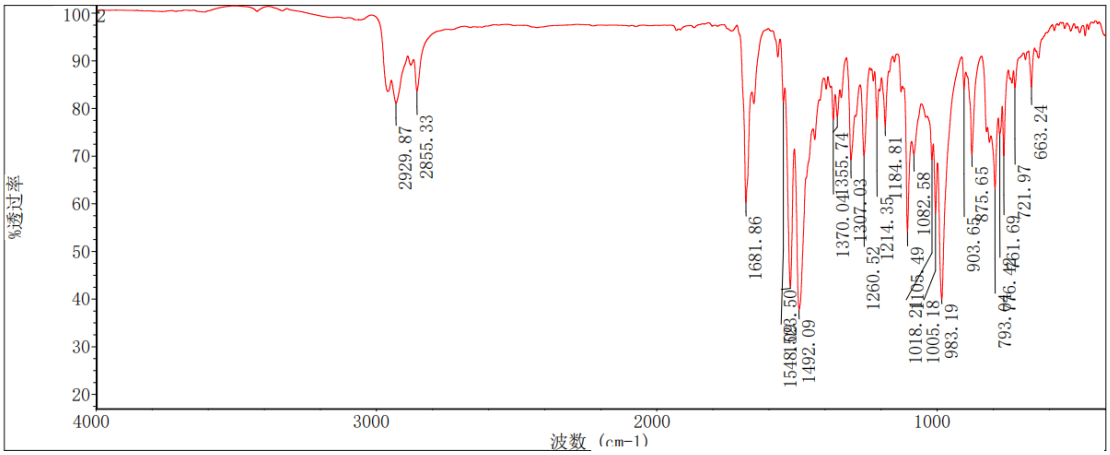

Figure S52. IR of compound **NP-CHO**.

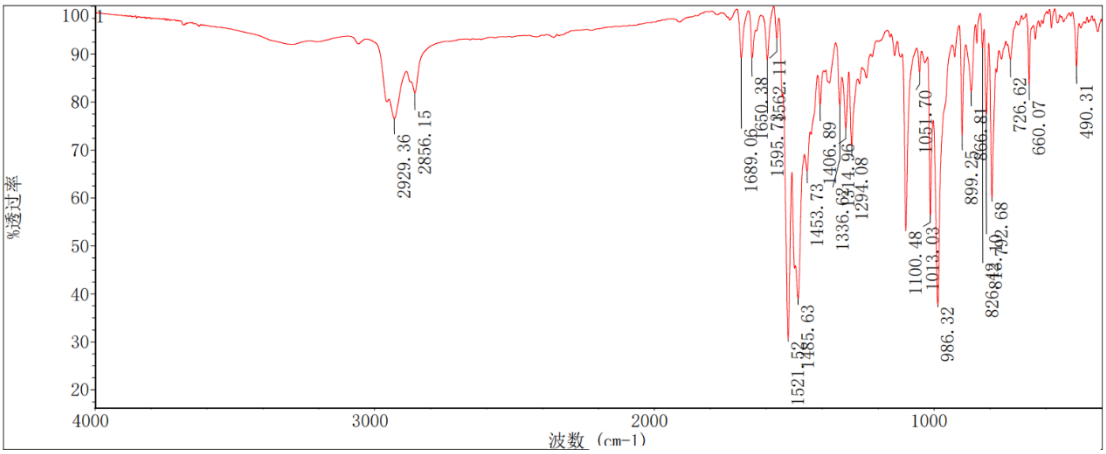

Figure S53. IR of compound **PerNN**.

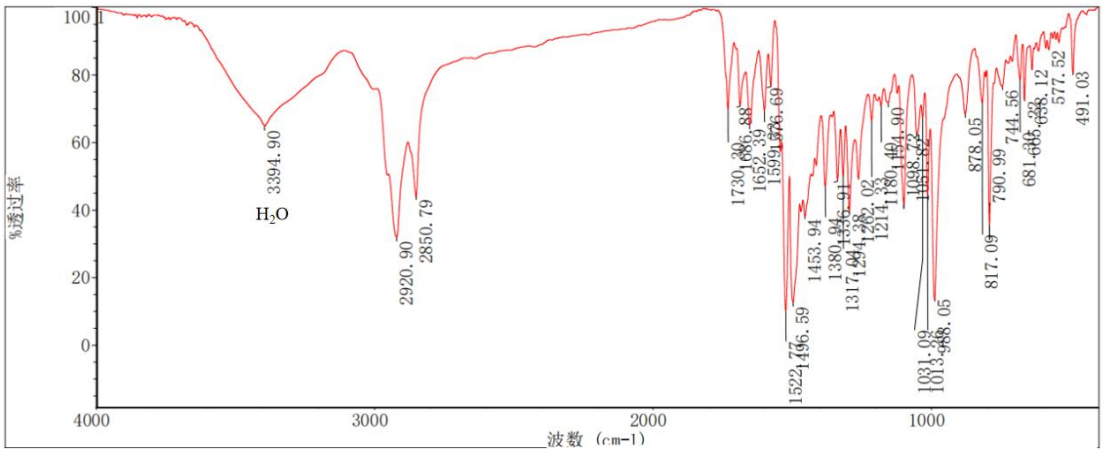

Figure S54. IR of compound **PerNN-MeI**.

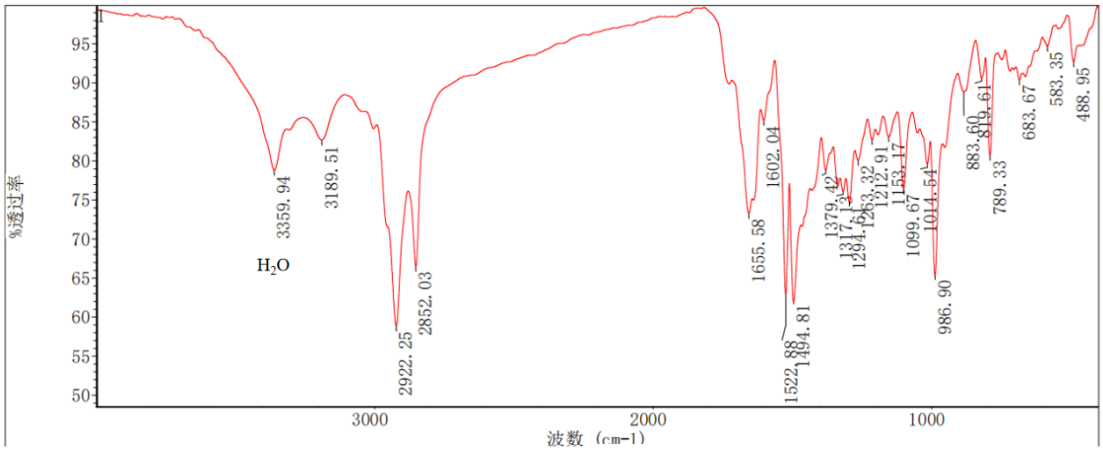

Figure S55. IR of compound **PerNN-MeCl**.

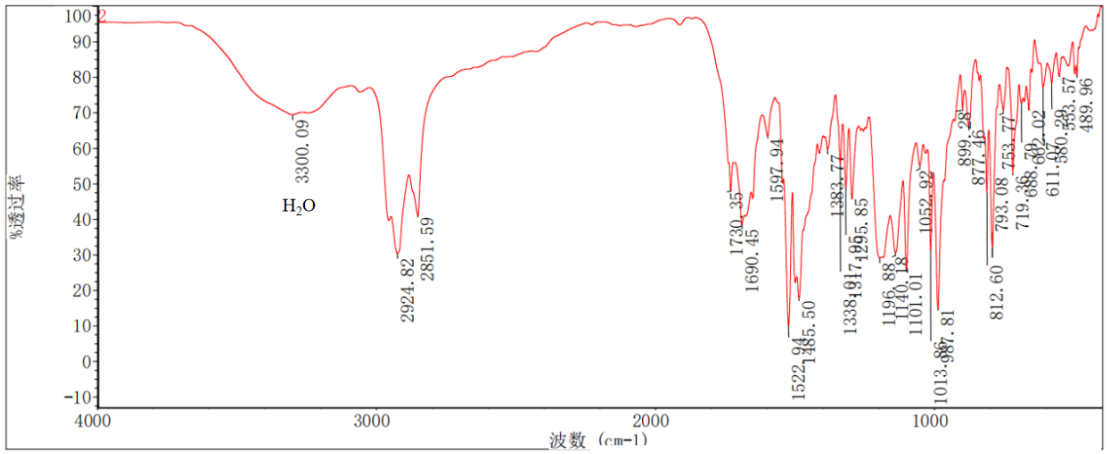

Figure S56. IR of compound **PerNN-H**.

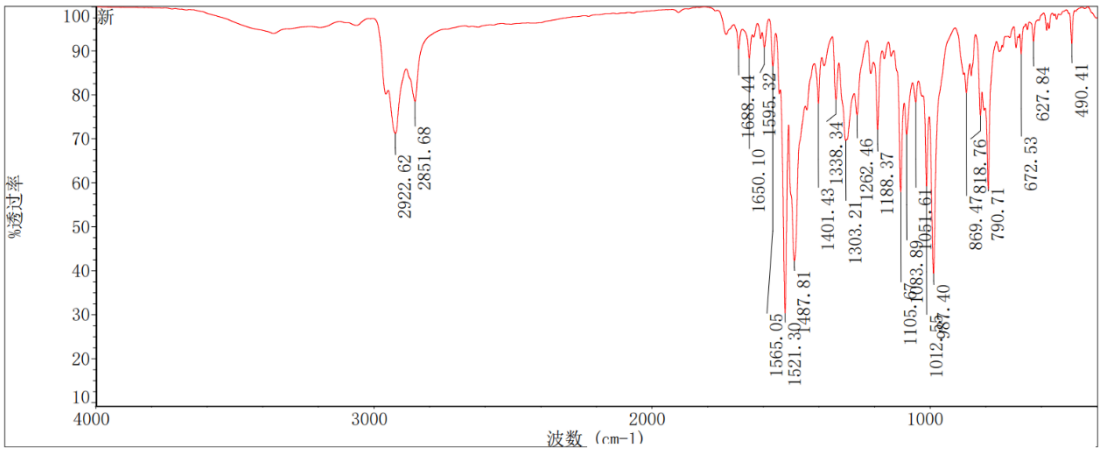

Figure S57. IR of compound **PerNN-O**.

7. Reference

[1] Zhang, W., Liu, G., Cao, J., Chen, Y., Gao, L., Liu, G., Dai G. and Wang, Q., Synthesis and Properties of BN-embedded N-Perylene. Chem. Asian J., **2022**, *17*, e202200340.

[2] Frisch, M. J., Trucks, G. W., Schlegel, H. B., Scuseria, G. E., Robb, M. A., Cheeseman, J. R., Scalmani, G., Barone, V., Petersson, G. A., Nakatsuji, H., Li, X., Caricato, M., Marenich A. V., Bloino, J., Janesko, B. G., Gomperts, R., B. Mennucci, B., Hratchian, H. P., Ortiz, J. V., Izmaylov, A. F., Sonnenberg, J. L., Williams-Young, D., Ding, F., Lipparini, F., Egidi, F., Goings, J., Peng, B., Petrone, A., T. Henderson, T., Ranasinghe, D., Zakrzewski, V. G., Gao, J., Rega, N., Zheng, G., Liang, W., Hada, M., Ehara, M., Toyota, K., R. Fukuda, R., Hasegawa, J., Ishida, M., Nakajima, T., Honda, Y., Kitao, O., Nakai, H., Vreven, T., Throssell, K., Montgomery, J. A., Peralta, J. E., Ogliaro, F., Bearpark, M. J., Heyd, J. J., Brothers, E. N., Kudin, K. N., Staroverov, V. N., Keith, T. A., Kobayashi, R., Normand, J., Raghavachari, K., Rendell, A. P., Burant, J. C., Iyengar, S. S., Tomasi, J., Cossi, M., Millam, J. M., Klene, M., Adamo, C., Cammi, R., Ochterski, J. W., Martin, R. L., Morokuma, K., Farkas, O., Foresman, J. B. and Fox, D. J., Gaussian, Inc., Wallingford CT, **2016**.

[3] Lu, T. and Chen, F. Multiwfn: A multifunctional wavefunction analyzer. J. Comput. Chem., **2012**, *33*, 580.

[4] Lu, T. and Chen, F. Quantitative analysis of molecular surface based on improved Marching Tetrahedra algorithm. J. Mol. Graph. Model., **2012**, *38*, 314.

[5] Humphrey, W., Dalke, A. and Schulten, K., VMD: visual molecular dynamics. J. Mol. Graph., **1996**, *14*, 33.

[6] Chen, Z., Wannere, C. S., Corminboeuf, C., Puchta, R., Schleyer, P. v. R. Nucleus-Independent Chemical Shifts (NICS) as an Aromaticity Criterion. Chem. Rev. **2005**, *105*, 3842.

[7] Geuenich D, Hess K, Köhler F, Herges R. Anisotropy of the induced current density (ACID), a general method to quantify and visualize electronic delocalization. Chem Rev. **2005**, *105*, 3758.